Coherent reflection in a two-dimensional cochlea: Short-wave versus long-wave scattering in the generation of reflection-source otoacoustic emissions

Christopher A. Shera[a)]
Eaton-Peabody Laboratory of Auditory Physiology, Massachusetts Eye and Ear Infirmary, 243 Charles Street, Boston, Massachusetts 02114 and Department of Otology and Laryngology, Harvard Medical School, Boston, Massachusetts 02115

Arnold Tubis
Department of Physics, Purdue University, West Lafayette, Indiana 47907 and Institute for Nonlinear Science, University of California—San Diego, La Jolla, California 92093

Carrick L. Talmadge
National Center for Physical Acoustics, University of Mississippi, University, Mississippi 38677

(Received 22 September 2004; revised 18 February 2005; accepted 1 March 2005)

The theory of coherent reflection filtering explains the empirical form of the cochlear reflectance by showing how it emerges from the coherent ''backscattering'' of forward-traveling waves by impedance perturbations in the mechanics of the cochlear partition. Since the theory was developed using the one-dimensional (1-D) transmission-line model of the cochlea, an obvious logical shortcoming is the failure of the long-wavelength approximation near the peak of the traveling wave, where coherent backscattering is purported to occur. Indeed, existing theory suggests that wave reflection may be strongly suppressed in the short-wave regime. To understand how short-wave behavior near the peak modifies the predictions of the long-wave theory, this paper solves the scattering problem in the 2-D cochlear model. The 2-D problem is reduced to a 1-D wave equation and the solution expressed as an infinite series in which successive terms arise via multiple scattering within the cochlea. The cochlear reflectance is computed in response-matched models constructed by solving the inverse problem to control for variations in mechanical tuning among models of different heights and dimensionality. Reflection from the peak region is significantly enhanced by the short-wave hydrodynamics, but other conclusions of the 1-D analysis—such as the predicted relation between emission group delay and the wavelength of the traveling wave—carry over with only minor modifications. The results illustrate the important role of passive hydromechanical effects in shaping otoacoustic emissions and cochlear tuning. [DOI: 10.1121/1.1895025]

PACS numbers: 43.64.Bt, 43.64.Kc, 43.64.Jb, 43.20.Bi [BLM] Pages: 287–313

I. INTRODUCTION

The theory of coherent reflection filtering describes the coherent backscattering of cochlear traveling waves by distributed mechanical perturbations within the organ of Corti. When combined with a description of sound transmission and reflection by the middle ear, the theory provides a comprehensive account of spontaneous and evoked otoacoustic emissions (OAEs) as well as the microstructure of the hearing threshold (e.g., Shera and Zweig, 1993b; Zweig and Shera, 1995; Talmadge *et al.*, 1998, 2000). Under conditions believed applicable at low and moderate sound levels, the theory predicts that the strongest backscattering occurs within the region about the peak of the traveling-wave envelope. For simplicity, the analysis of cochlear wave reflection that supports this conclusion was performed using the one-dimensional (long-wave) model of the cochlea. An obvious technical defect of this approach, however, is the breakdown of the long-wave assumption in the region near the peak of the traveling wave.

Validity of the long-wave assumption requires that the wavelength λ of the traveling wave be large compared to the dimensions of the scalae. A rough guideline specifies that $\lambda > 2\pi H$, where H is the height (or radius) of the cochlear duct (e.g., Lighthill, 1981; de Boer, 1996). Although the long-wave approximation is believed valid in the basal-most ''tail'' region of the cochlear response where OAEs couple to the middle ear (e.g., Nedzelnitsky, 1980), in the peak region the wavelength of the traveling wave is smaller than the dimensions of the scalae, and the short-wave model is more appropriate. For example, Fig. 1 shows estimates of the ratio $kH \equiv 2\pi H/\lambda$ evaluated at the peak of the traveling wave for both human and guinea pig. Although the values are only approximate, the conclusion is clear: Except perhaps in the apex of the guinea-pig cochlea, the long-wave assumption is everywhere violated at the peak of the traveling wave (see also de Boer, 2001). Since the long-wave assumption fails in precisely the region where coherent backscattering is pre-

a)Electronic mail: shera@epl.meei.harvard.edu

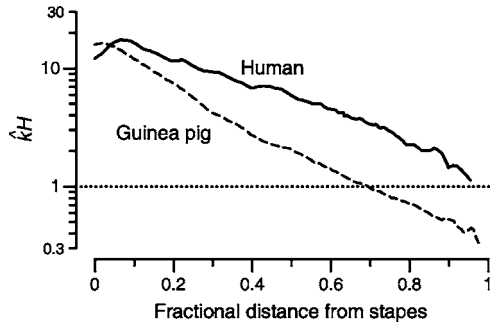

FIG. 1. Violation of the long-wave assumption at the peak of the traveling wave. The figure shows estimates of $\hat{k}H \equiv 2\pi H/\hat{\lambda}$ for the human (solid line) and guinea pig (dashed line) versus fractional distance from the stapes. The wavelength $\hat{\lambda}$ is evaluated at the peak, $\hat{x}(\omega)$, of the traveling wave envelope. For each species, the scala height H was defined as the radius of the equivalent circle (area equal to the combined areas of the scala vestibuli and tympani) as computed from measured scalae dimensions (Thorne *et al.*, 1999). Estimates of $\hat{\lambda}$ were obtained from otoacoustic measurements of stimulus-frequency emission (SFOAE) group delay transformed into equivalent wavelengths using local scaling symmetry and the cochlear map (Shera and Guinan, 2003, Table II). Cochlear maps were adjusted so that the total cochlear length matched the values reported by Thorne *et al.* (1999). Values of $\hat{k}H$ greater than 1 (dotted line) are inconsistent with the long-wave assumption.

dicted to occur, conclusions based on the one-dimensional analysis about the strength and character of wave reflection remain of uncertain validity.

Interestingly, the literature suggests that wave reflection may indeed differ profoundly in long- and short-wave cochlear models. For example, in Siebert's classic formulation of the short-wave model, waves propagating in the two directions satisfy a pair of first-order differential equations, each of which has an exact closed-form solution (e.g., Siebert, 1974; de Boer, 1979, 2001). Siebert's equations for the waves traveling in the two directions are uncoupled, suggesting that wave reflection (e.g., due to rapid spatial variations in the partition impedance) does not occur in a short-wave cochlea (e.g., de Boer, 1983). Zwislocki (1983, 2002) arrives at the same conclusion by an entirely different route. By transforming long- and short-wave models into equivalent transmission lines and analyzing their characteristic impedances, Zwislocki constructs an "unequivocal ... proof" that cochlear wave reflection, although inevitable in the long-wave model, cannot occur in the short-wave regime.

The apparent absence of reflections in the short-wave model has been invoked to explain a puzzle of mammalian cochlear anatomy:[1] Since so much of the important hydromechanical action in the cochlea appears confined to the immediate vicinity of the cochlear partition (e.g., Olson, 2001), why do the scalae vestibuli and tympani grow considerably larger than seems necessary to house the organ of Corti? Because the presence of large reverse-traveling waves would presumably complicate the detection and analysis of sound, perhaps the scalae have evolved their present sizes, so the argument goes, because the hydrodynamics in the peak region need to be short-wave in order to suppress the reflection of traveling waves. If these ideas are correct, and scattering off perturbations in the short-wave region near the peak of the traveling wave is significantly suppressed, or perhaps even nonexistent, then current understanding of OAE generation needs substantial revision.

However, careful examination of the arguments against short-wave reflection suggests that the jury may still be out. Zwislocki's proof, for example, hinges on the validity of his demonstration that in the short-wave limit the characteristic impedance of the equivalent transmission line becomes independent of the partition impedance. But so counter-intuitive is this result that corollary conclusions about wave reflection are hard to credit without independent corroboration. Although Siebert's uncoupled equations might be cited in this regard, closer inspection reveals that they offer no compelling assurances. As Siebert himself makes clear, the derivation of his equations hinges on assumptions that are violated in the presence of irregular perturbations ("roughness") in the mechanics. In particular, Siebert (unlike Zwislocki) assumes that the mechanics of the partition vary so smoothly with position that spatial-frequency components in the partition impedance that unnecessarily complicate his analysis by coupling forward- and reverse-traveling waves can safely be neglected. Without this explicit assumption of mechanical smoothness—an assumption manifestly invalid in the presence of roughness—Siebert's neat decoupling of forward and reverse waves cannot be obtained. Consequently, Siebert's equations cannot be used to understand the nature of wave reflection in the short-wave regime. Although de Boer (2001) has shown that Siebert's two first-order equations can be combined into a single second-order equation that supports both forward- and reverse-traveling waves—and, by implication, the possibility of internal reflection—the procedure remains grounded on equations that apply only in the absence of mechanical perturbations.

The analysis of cochlear wave reflection clearly requires a theory of wave scattering valid in the short-wave regime. Unfortunately, current understanding appears doubly unsatisfactory, for the relevant theories appear mutually exclusive, with no obvious overlapping regions of validity. Whereas the theory of coherent reflection was developed using assumptions about cochlear hydrodynamics that break down in the short-wave regime purported to encompass the region of maximal scattering, the classic theory of the short-wave regime relies on assumptions about the mechanics that fail in the presence of perturbations that might scatter the wave. In this paper, we resolve the dilemma by developing a cochlear scattering formalism for a two-dimensional cochlear model that supports both long and short waves and the transition between the two. Our analysis makes no implicit smoothness assumptions and remains valid in the presence of mechanical perturbations. We apply the formalism to investigate whether—and if so how—the predictions of the long-wave theory of reflection-source OAEs change when the modeling framework is extended to capture the short-wave behavior near the peak of the traveling wave.

Overview

Our argument has three parts and a prologue. After perusing this synopsis, readers interested primarily in the conclusions rather than their logical justification might skip

ahead to part three (Sec. VI) on the assumption that all's well that ends well. For reference, Appendix E contains a list of frequently used symbols.

Preparatory to anything else we begin by reviewing relevant assumptions and deriving the equations for a two-dimensional (2-D) cochlear model with mechanical perturbations (or roughness) in the partition (Sec. II). Our goal is to understand the effects of long- versus short-wave scattering on the properties of reflection-source OAEs. Since bidirectional coupling between the ear canal and the basal, long-wave region of the cochlea is well described by 1-D theory (e.g., Nedzelnitsky, 1980; Shera and Zweig, 1992a; Talmadge *et al.*, 1998; Puria, 2003), our concern here is only to understand the physics that gives rise to reverse-traveling waves within the cochlea (i.e., the mechanisms of emission generation). As viewed from the stapes, backscattering of traveling waves manifests itself as a nonzero value of the cochlear reflectance, R, defined as the ratio of the outgoing to the ingoing pressure waves at the stapes. Our strategy is therefore to calculate R in models of different heights or dimensionality.

The first part of the argument then begins in Sec. III, where we show how the general 2-D problem can be reduced to a 1-D wave equation by considering the pressure averaged over the scalae area, as originally suggested by Duifhuis (1988; see also Zwislocki, 1953). At the base of the cochlea this averaged pressure determines the net force on the stapes and therefore controls how OAEs couple to the middle ear. Traveling-wave solutions in the smooth cochlea permit the definition of "projection operators" that decompose the averaged pressure into components representing forward- and reverse-traveling waves. By introducing the scalae-averaged response to an oscillating point source located on the BM (the "reduced traveling-wave Green's function"), we then show that the model solution in the presence of perturbations takes the form of an infinite series in which successive terms arise physically via multiple wave scattering within the cochlea (Sec. IV). We derive an approximate expression for the reduced traveling-wave Green's function valid in the "far field" at some distance from the source (e.g., near the stapes). Using the projection operators to extract the wave components then yields a first-order perturbative expression for the cochlear reflectance, R.

In the second part we argue that comparing values of R calculated in models of different heights requires compensating for variations in mechanical tuning that would otherwise arise were the BM impedance function held constant (Sec. V). To control for variations in tuning we need to find the BM impedance that yields a given velocity response in a model of specified height, and we develop a new method for solving this cochlear "inverse problem."

In the third and final part we bring everything together and compute the cochlear reflectance in response-matched 1-D and 2-D models of various heights (Sec. VI). We use the results to compare and contrast the nature of wave scattering in long- and short-wave models. We find that the reflection from the peak region—rather than being reduced or even eliminated relative to the long-wave case, as suggested by Zwislocki's analysis—is actually enhanced in the short-wave regime. In effect, the hydrodynamics of the short-wave regime act to magnify the effective size of the perturbations located within the peak of the traveling wave. In other respects, however, the principal conclusions of the 1-D analysis—such as the predicted relation between emission group delay and the wavelength of the traveling wave—survive with only minor modification.

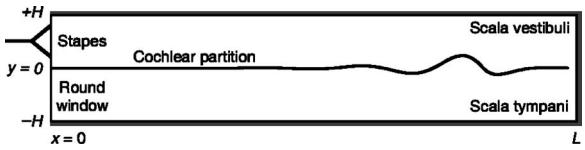

FIG. 2. Sagittal spacetime slice through the two-dimensional box model. The scala vestibuli and scala tympani are assumed to have equal rectangular cross sections of height H. In the z direction perpendicular to the page the width of the scalae is assumed to be everywhere much less than a wavelength so that the model is effectively two dimensional. The cochlear partition, schematized here as a thin membrane partaking in a traveling wave, manifests micromechanical impedance perturbations arising from its discrete cellular architecture. Note that the partition displacement has been grossly exaggerated to make the wave visible on the scale of the figure.

II. A TWO-DIMENSIONAL COCHLEA WITH PERTURBATIONS

A. Assumptions of the model

For clarity of exposition, we make several simplifying assumptions in order to eliminate technical complications that obscure the most important points of the analysis.

First and foremost, we work with the simplest geometry that manifests both long- and short-wave behavior. In particular, we assume a linear, two-dimensional box model of the cochlea with incompressible and inviscid scala fluids (see Fig. 2). The x axis extends longitudinally from the base ($x=0$), and the y axis is oriented perpendicular to the basilar membrane (BM), which is located in the xz plane and spans the entire width, b, of the cochlea (a configuration de Boer has referred to as "wall-to-wall carpeting" with a stereociliary shag). Except at the two windows, we assume that the box is surrounded by rigid bone so that no net fluid enters or leaves the cochlea at acoustic frequencies; the volume displacements of the two windows are therefore equal and opposite.

In the 1-D model, the wavelengths of the waves on the cochlear partition are assumed to be large relative to the heights (and widths) of the scalae so that the pressures and fluid velocities are nearly uniform in any "radial" cross section parallel to the yz plane. Here, we relax this "long-wavelength" assumption and allow the dynamical variables to depend on y, the height above the partition. Effectively, we assume that the width b of the BM—but not necessarily the height H of the scalae—is everywhere much less than a wavelength. Since the pressure field is assumed to be independent of z, the problem is $2+1$ dimensional (2 space, 1 time).

We neglect possible complex spatial variations in the pressure in the immediate vicinity of the oval and round windows at $x=0$; in effect, we assume that the two windows move as rigid pistons with areas that match those of their respective scalae. Furthermore, we assume that the cochlea is

effectively semi-infinite in extent (or, equivalently, that stimulus frequencies are not so low that reflections from the helicotrema and the apical wall contribute significantly to the response). Thus, the only source of apical cochlear wave reflections that we consider is BM roughness, whose perturbative effects are discussed in Sec. IV.

Since the model is linear, its response to any stimulus is completely determined by its response to pure tones. We therefore assume harmonic time dependence and write pressures, velocities, and other dynamical variables as complex Fourier amplitudes representing responses at angular frequency ω [e.g., $v_{\mathrm{BM}}(x,t)=\mathrm{Re}\{V_{\mathrm{BM}}(x,\omega)e^{i\omega t}\}$], where ω is 2π times the stimulus frequency, f. Fourier transformation converts the third (temporal) dimension to frequency; for notational simplicity, we usually leave the functional dependence on frequency implicit and refer to the model as two-dimensional (2-D).

The pressure field in the cochlea can be separated into terms symmetric and antisymmetric about the BM (sum and difference pressures, respectively). Since the two model scalae are symmetric about the BM, the sum and difference pressures are decoupled. We assume that the cochlear partition responds only to the pressure difference across its surface (e.g., Voss *et al.*, 1996), and not to the absolute pressure within the scalae; consequently, we need only consider the pressure difference $P(x,y)$ that gives rise to the classical traveling wave. The difference pressure is defined by $P(x,y)\equiv p(x,y)-p(x,-y)$, where $p(x,y)$ is the scala pressure (i.e., the scala-vestibuli pressure for $y>0$ and the scala-tympani pressure for $y<0$). The pressure difference is antisymmetric about the partition: $P(x,-y)=-P(x,y)$.

B. Synopsis of the model equations

With the exception of an explicit consideration of perturbations in the mechanics of the partition, the equations and boundary conditions describing the model are completely standard (for reviews see Viergever, 1980; de Boer, 1996). All equations follow immediately from Newton's laws; we catalog them here in order to introduce our notation.

Fluid dynamics and boundary conditions. The linearized Euler equation (Newton's second law) and the assumed incompressibility of the cochlear fluids together imply that the pressure difference $P(x,y)$ satisfies Laplace's equation,

$$\nabla^2 P(x,y)=(\partial_x^2+\partial_y^2)P=0, \tag{1}$$

where we have adopted the notational shorthand $\partial_x\equiv\partial/\partial x$. Since the scalae walls are assumed rigid, the normal component of the fluid velocity, and hence the corresponding component of the pressure gradient, must vanish at $y=\pm H$:

$$\partial_y P|_{y=\pm H}=0. \tag{2}$$

Just above the cochlear partition, the fluid velocity must equal the velocity of the BM. Thus,

$$\partial_y P|_{y=0^+}=2i\omega\rho_0 V_{\mathrm{BM}}, \tag{3}$$

where ρ_0 is the density of the cochlear fluids and positive BM displacements are those produced (at $t=0^+$) by positive displacements of the stapes (i.e., positive *into* the scala tympani).

Coupling with the middle ear. Just inside the oval window the x (or longitudinal) component of the fluid velocity must equal the velocity of the stapes. Consequently,

$$U_{\mathrm{sv}}(0)=U_{\mathrm{ow}}, \tag{4}$$

where U_{ow} is the volume velocity of the oval window; $U_{\mathrm{sv}}\equiv\mathbf{U}_{\mathrm{sv}}\cdot\mathbf{e}_x$, with $\mathbf{e}_x$ denoting the unit vector in the longitudinal direction; and $\mathbf{U}_{\mathrm{sv}}(x)$, the scala-vestibuli volume velocity, is given in terms of the fluid particle velocity, $\mathbf{u}_{\mathrm{sv}}(x,y)$, by

$$\mathbf{U}_{\mathrm{sv}}(x)\equiv b\int_0^H \mathbf{u}_{\mathrm{sv}}(x,y)dy. \tag{5}$$

Analogous expressions hold for the longitudinal component of the scala-tympani volume velocity, $U_{\mathrm{st}}(x,y)$.

Equation (4) can be expressed in terms of the pressure by integrating the linearized Euler equation over the scalae to obtain

$$\partial_x\bar{P}=-Z_{\mathrm{f}}U, \tag{6}$$

where $U\equiv(U_{\mathrm{sv}}-U_{\mathrm{st}})/2$ and the average pressure $\bar{P}(x)$ is defined by

$$\bar{P}(x)\equiv\frac{1}{H}\int_0^H P(x,y)dy. \tag{7}$$

The impedance Z_{f} is defined by

$$Z_{\mathrm{f}}\equiv 2i\omega\rho_0/S, \tag{8}$$

where $S\equiv bH$ is the scala area. Z_{f} has units of acoustic impedance per unit length and characterizes the effective acoustic mass of the fluids. Because the cochlear contents and their bony enclosure have been assumed incompressible, $U_{\mathrm{sv}}+U_{\mathrm{st}}=0$ (e.g., Shera and Zweig, 1992b); consequently $U\equiv(U_{\mathrm{sv}}-U_{\mathrm{st}})/2=U_{\mathrm{sv}}$. The stapes boundary condition [Eq. (4)] therefore becomes

$$\partial_x\bar{P}|_{x=0}=-Z_{\mathrm{f}}U_{\mathrm{ow}}. \tag{9}$$

Since our focus here is the physics of wave scattering in the cochlea, we do not employ equations relating intracochlear pressures to those measured in the ear canal. At frequencies well below the maximum characteristic frequency of the partition, the coupling of OAEs into the middle ear involves pressures in the long-wave regime, and the 1-D theory remains valid even if the peak region is short wave. Equations describing sound transmission and reflection by the middle ear are discussed elsewhere (e.g., Shera and Zweig, 1992a,c; Peake *et al.*, 1992; Talmadge *et al.*, 1998; Schairer *et al.*, 2003). Here, we characterize the mechanical and acoustical effects of the external world seen from the cochlea, including the middle ear and any sound sources in the ear canal, by their Thévenin-equivalent source pressure and impedance (e.g., Beranek, 1986). The Thévenin-equivalent impedance can in turn be represented as an equivalent reflection coefficient, R_{stapes}, characterizing the reflection of reverse-traveling waves incident upon the stapes (e.g., Carlin and Giordano, 1964; Shera and Zweig, 1991; Talmadge *et al.*, 1998).

Dynamics of the cochlear partition. The cochlear partition is represented by an effective point impedance function that characterizes the motion induced by the pressure difference across its surface. $\tilde{Z}_{\mathrm{BM}}(x)$ is defined by

$$\tilde{Z}_{\mathrm{BM}}(x) \equiv \frac{P(x,0^+)}{bV_{\mathrm{BM}}(x)}. \tag{10}$$

We have included the factor of b in the definition, thereby giving the impedance units of acoustic impedance times length, so that it matches the definition employed in the 1-D transmission-line model. As explained below, the diacritical tilde indicates the presence of mechanical perturbations. When rewritten in terms of the BM impedance, the BM boundary condition [Eq. (3)] assumes the form

$$\partial_y \ln P\big|_{y=0^+} = \frac{2i\omega\rho_0}{b\tilde{Z}_{\mathrm{BM}}} = HZ_{\mathrm{f}}/\tilde{Z}_{\mathrm{BM}}(x). \tag{11}$$

Note that we have left the functional form of $\tilde{Z}_{\mathrm{BM}}(x)$ completely unspecified. In order to provide a concrete example, we later determine the BM impedance by requiring that the model reproduce a given BM velocity response.

Perturbations in the mechanics. At the micromechanical level, the properties of the cochlear partition presumably vary somewhat irregularly with position (e.g., due to spatial variations in the number, geometry, or mechanical characteristics of the outer hair cells). This micromechanical "roughness" appears superimposed on an overall smooth variation of the mechanics responsible for such things as the cochlear mapping between frequency and position. We represent these micromechanical irregularities as small perturbations, $\Delta Z_{\mathrm{BM}}(x)$, in the impedance of the partition. To indicate that the impedance includes perturbations arising from irregularities in the mechanics, we write $\tilde{Z}_{\mathrm{BM}}(x)$ with a diacritical tilde. Thus,

$$\tilde{Z}_{\mathrm{BM}}(x) = Z_{\mathrm{BM}}(x) + \Delta Z_{\mathrm{BM}}(x), \tag{12}$$

where $Z_{\mathrm{BM}}(x)$ is the "smooth" component of the impedance obtained by "ironing out" the perturbations ΔZ_{BM}.

C. Statement of the problem

Otoacoustic emissions are presumed to indicate the presence of reverse-traveling pressure waves within the cochlea. In a linear cochlea, these waves manifest themselves in the ear canal via their effect on the cochlear input impedance. As discussed in detail elsewhere (e.g., Shera and Zweig, 1993a; Zweig and Shera, 1995; Talmadge *et al.*, 1998), the problem boils down to computing the value of the cochlear reflectance, defined by

$$R \equiv \left.\frac{\bar{P}_l}{\bar{P}_r}\right|_{x=0}, \tag{13}$$

where $\bar{P}_{\{r,l\}}$ are the forward- and reverse-traveling components of the pressure $\bar{P}$ influencing the motion of the stapes. The subscripts $\{r,l\}$ designate waves traveling to the "right" and to the "left," respectively, consistent with the cochlear orientation illustrated in Fig. 2.

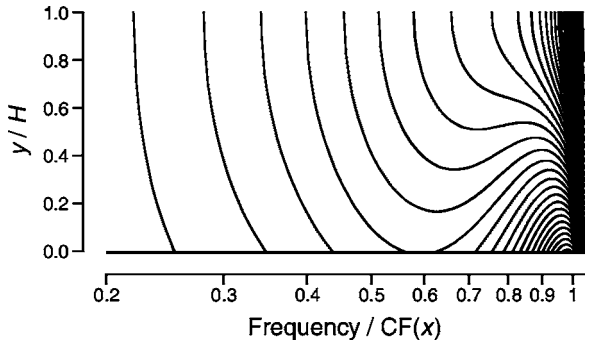

FIG. 3. Amplitude of the pressure field $P(x,y)$ in the scala vestibuli ($y>0$) for a 2-D model cochlea driven from the stapes with a pure-tone stimulus of frequency f. The spatial coordinate x varies along the abscissa and is shown in the form $f/\mathrm{CF}(x)$ so that the peak of the corresponding BM velocity response occurs at the value 1. The y coordinate is normalized by the model height, H (0.7 mm). The BM is represented by the line located along the bottom edge of the plot ($y=0$). Iso-pressure contours are spaced at intervals of 1 dB. The model's BM impedance function, with parameters chosen so that $\hat{k}H \cong 6$ (detailed in Appendix D, Table I), derives from the inverse solution of Zweig (1991) and varies smoothly with position ($\epsilon=0$). $P(x,y)$ was computed numerically using finite differences (e.g., Neely, 1981).

In a nutshell, the problem is to solve Eq. (1) for the pressure $P(x,y)$—subject to boundary conditions at the cochlear walls, stapes, and BM [Eqs. (2), (9), and (11)]—in order to determine how mechanical perturbations $\Delta Z_{\mathrm{BM}}(x)$ affect the cochlear response. By analogy with the scattering of light (e.g., by smoke or density fluctuations in the atmosphere), we expect the perturbations to "scatter" incident traveling waves back toward the stapes, where they contribute to the cochlear reflectance, R. This "scattering problem" has been solved for the 1-D long-wave model (Zweig and Shera, 1995; Talmadge *et al.*, 1998), and our purpose here is not merely to repeat the derivation in 2-D. Rather, our goal is to understand how the results depend on the short- or long-wave behavior of the model, that is, on the value of $\hat{k}H$, where $\hat{k}$ denotes the (real^2) wave number at the peak ($\hat{x}$) of the traveling wave, $\hat{k} \equiv k[\hat{x}(\omega),\omega]$. The character of the waves in the peak region varies inversely with $\hat{k}H$: when $\hat{k}H$ is small, the waves are long wave; when $\hat{k}H$ is large, the waves are short wave. In all cases we assume that the basal-most "tail" region of the cochlear response remains long wave ($k_0 H \ll 1$). This assumption is consistent with pressure measurements made in the basal region of the cochlea, which indicate that at frequencies well below the maximum characteristic frequency of the partition the wavelength of the cochlear traveling wave is large compared to the dimensions of the scalae (e.g., Nedzelnitsky, 1980).

Figure 3 illustrates these remarks by showing the pressure field $P(x,y)$ produced by a pure-tone stimulus in an active 2-D model of the cochlea with parameters chosen so that $\hat{k}H \cong 6$. (Appendix D provides details of the model and a synopsis of our numerical procedures, including the checks used to ensure integrity of the solution.) The iso-pressure contours, spaced at intervals of 1 dB, show that the pressure remains nearly uniform across the scalae in the basal-most tail region near the stapes but becomes highly nonuniform near the characteristic place, where the largest pressures are

found in the immediate vicinity of the BM (cf. Olson, 2001).

To explore the effects of perturbations in the mechanics we could simply assume some convenient form for $\tilde{Z}_{\mathrm{BM}}(x)$ and solve the model equations numerically, as we did for a model without perturbations in Fig. 3. However, understanding any differences between short- and long-wave scattering requires a more considered approach. As we will see, straightforward numerical simulations, if naively interpreted, can introduce spurious sources of variation that seriously compromise the analysis of short- versus long-wave scattering.

III. REDUCTION TO A ONE-DIMENSIONAL WAVE EQUATION

The derivation of a perturbative theory of coherent wave reflections in the 1-D framework is greatly simplified by the existence of an inhomogeneous one-dimensional wave (Helmholtz) equation for the pressure (e.g., Zweig and Shera, 1995; Talmadge *et al.*, 1998). We now derive a generalization of this equation for a 2-D model, based on the work of Duifhuis (1988; Talmadge *et al.*, 2001).

Otoacoustic emissions originating in the cochlea are manifest in the ear canal because of their coupling through the middle ear. As outlined above, this coupling depends on the pressure averaged over the stapes footplate. Our strategy is therefore to consider the quantity $\bar{P}(x)$, defined by Eq. (7) and reproduced below:

$$\bar{P}(x) \equiv \frac{1}{H}\int_0^H P(x,y)\,dy. \tag{14}$$

An equation for $\bar{P}(x)$ can be obtained by averaging $\nabla^2 P$ [Eq. (1)] over the upper duct and applying boundary conditions at the BM and $y=H$ [Eqs. (2) and (11)]. The result is

$$\partial_x^2 \bar{P} + \tilde{k}_{\mathrm{lw}}^2 P_0 = 0, \tag{15}$$

where

$$P_0(x) \equiv P(x,0^+). \tag{16}$$

The function $\tilde{k}_{\mathrm{lw}}(x)$ is given by

$$\tilde{k}_{\mathrm{lw}}^2(x) \equiv -Z_{\mathrm{f}}/\tilde{Z}_{\mathrm{BM}}(x), \tag{17}$$

where the fluid impedance Z_{f} is defined by Eq. (8).

Following Duifhuis (1988) we now introduce the function $\alpha(x)$, defined by

$$\alpha(x) \equiv \frac{P_0(x)}{\bar{P}(x)}. \tag{18}$$

At every location x the function $\alpha(x)$ is the ratio of the pressure driving the cochlear partition to the pressure averaged over the scalae cross section. The value of $\alpha(x)$ depends on the effective dimensionality of the fluid flow at location x. Since the largest pressures are found close to the partition, $|P_0| \geqslant |\bar{P}|$ so that $|\alpha| \geqslant 1$ in the traveling-wave region of the cochlea basal to $\hat{x}(\omega)$. To provide a concrete example, Figs. 4 and 5 show plots of $P_0(x)$, $\bar{P}(x)$, and their ratio, $\alpha(x)$, computed from the pressure field $P(x,y)$ produced by sinusoidal stimulation at the stapes (Fig. 3).

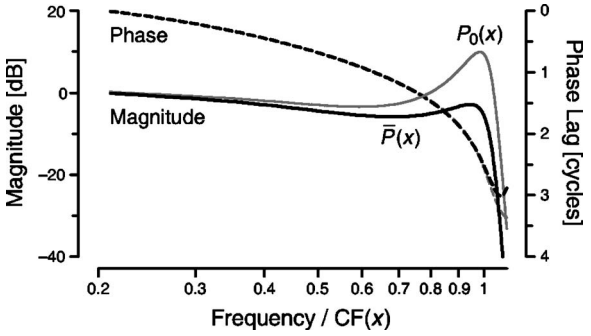

FIG. 4. $P_0(x)$ and $\bar{P}(x)$ computed from the pressure field shown in Fig. 3. Magnitudes (solid lines) are shown in dB (left-hand scale). Phases (dashed lines) are shown in cycles (right-hand scale). Both magnitude and phase are plotted relative to the value of $\bar{P}(0)$.

Rewriting Eq. (15) for $\bar{P}$ using Eq. (18) for α we find that the average pressure $\bar{P}(x)$ satisfies the one-dimensional wave equation

$$(\partial_x^2 + \tilde{k}^2)\bar{P} = 0, \tag{19}$$

where the complex-valued wave number, $\tilde{k}(x)$, is given by

$$\tilde{k}^2(x) \equiv \alpha(x)\tilde{k}_{\mathrm{lw}}^2(x) = -\alpha(x) Z_{\mathrm{f}}/\tilde{Z}_{\mathrm{BM}}(x). \tag{20}$$

Note that $\tilde{k} \to \tilde{k}_{\mathrm{lw}}$ in the long-wave regime where $\alpha \to 1$. For future convenience we write $\tilde{k}^2$ in the form

$$\tilde{k}^2(x) = k^2(x)[1+\epsilon(x)], \tag{21}$$

where $\epsilon(x)$ is related to the perturbations ΔZ_{BM} through the equation $\epsilon = -\delta/(1+\delta)$, with $\delta \equiv \Delta Z_{\mathrm{BM}}/Z_{\mathrm{BM}}$.

Character of the solution in the smooth cochlea

Before pursuing the effects of perturbations, we first explore the character of the solution in the smooth cochlea obtained by taking $\epsilon \to 0$, a process equivalent to ironing out the mechanical perturbations to recover the smooth wave number, $k(x)$. In the smooth cochlea Eq. (19) becomes

$$(\partial_x^2 + k^2)\bar{P} = 0. \tag{22}$$

Because the average pressure $\bar{P}(x)$ satisfies a one-dimensional wave equation, we expect the general solution

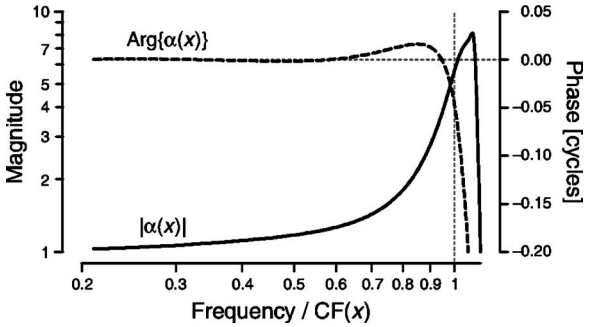

FIG. 5. The function $\alpha(x)$ defined as the ratio $P_0(x)/\bar{P}(x)$ computed from values shown in Fig. 4. Magnitude and phase scales are shown on the left- and right-hand sides of the plot, respectively. For reference, a horizontal dotted line intersects the phase ordinate at 0 cycles. A vertical dotted line locates the peak of the corresponding BM velocity response along the abscissa.

to comprise a superposition of waves traveling in opposite directions with local wavelength $\lambda(x)=2\pi/k(x)$. For example, in the long-wave regime $\alpha\to 1$ and thus $k\to k_{\mathrm{lw}}$. In this regime the impedance $Z_{\mathrm{BM}}(x)$ is dominated by the stiffness of the partition and the wave number $k\cong k_{\mathrm{lw}}$ is therefore essentially real. Equation (22) for $\bar{P}(x)$ thus has the standard Sturm-Liouville form so that its solutions can be presumed oscillatory (e.g., Ince, 1956; Courant and Hilbert, 1953); appropriate linear combinations can then be formed that represent waves traveling independently in opposite directions. Note, however, that the traveling-wave solutions for $\bar{P}(x)$ deduced from Eq. (22) are, at this point, only formal: Eq. (20) indicates that the wave number $k(x)$ depends on $\alpha(x)$, which remains undetermined except in the long-wave regime, where $\alpha\to 1$.

Duifhuis' (1988) procedure for reducing Eq. (15) to a one-dimensional wave equation can only be useful for investigating the reflection of cochlear traveling waves if the process is more than clever sleight-of-hand [for a review, see Jay (2001)]. In particular, the reduction must hold—with the same value of $\alpha(x)$—for waves traveling in both directions. We argue that this is true on general grounds.[3] Suppose we find a solution $P(x,y)$ to the model equations corresponding to a forward-traveling wave. For example, $P(x,y)$ can be computed numerically when the model is driven from the stapes (e.g., Fig. 3). In the basal, long-wave region of the cochlea, the solution will match the standard, one-dimensional solution for a forward-traveling wave. From the solution $P(x,y)$ we can compute the corresponding values of $\alpha(x)$ and $k(x)$, and we will find that the average pressure $\bar{P}(x)$ satisfies Eq. (22) exactly throughout the cochlea. But Eq. (22) is a second-order equation, and it therefore has another, independent solution with the same values of $k(x)$ and $\alpha(x)$. This additional solution has the form of a reverse-traveling wave; like the forward-traveling wave, it transforms smoothly into the standard long-wave solution in the basal region near the stapes.

IV. SOLVING FOR THE COCHLEAR REFLECTANCE

A. Basis waves and projection operators

The two independent traveling-wave solutions in the smooth cochlea constitute "basis waves" that define what is meant by forward- and reverse-traveling waves in a nonuniform medium (Shera and Zweig, 1991; Talmadge *et al.*, 1998). The basis waves, here denoted $W_{\{r,l\}}(x)$, are solutions of the homogeneous wave equation

$$(\partial_x^2+k^2)W_{\{r,l\}}=0. \tag{23}$$

By convention, the basis waves are dimensionless and are normalized so that $W_{\{r,l\}}(0)=1$. Their form can be obtained numerically or analytically using the WKB approximation. In Appendix A we present a procedure for suppressing reflection at the stapes in order to obtain pure forward- and reverse-traveling numerical solutions. We also derive approximate basis waves using the WKB approximation and show that they provide better solutions to Eq. (23) than those obtained from the "standard" WKB solutions for the 2-D model (e.g., Steele and Taber, 1979; Viergever, 1980; de Boer and Viergever, 1982).

The basis waves are central to our analysis because they allow the definition of "projection operators," $\hat{P}_{\{r,l\}}$, that decompose the total pressure at any point into components representing forward- and reverse-traveling waves.[4] The projection operators are defined so that

$$\bar{P}_{\{r,l\}}(x)=\hat{P}_{\{r,l\}}\{\bar{P}(x)\}; \tag{24}$$

they are given in terms of the basis waves $W_{\{r,l\}}(x)$ by the formula (Shera and Zweig, 1991)

$$\hat{P}_{\{r,l\}}=\pm\gamma W_{\{r,l\}}[\partial_x W_{\{l,r\}}-W_{\{l,r\}}\partial_x], \tag{25}$$

where the complex constant γ is the reciprocal of the Wronskian determinant [Eqs. (B5) and (B7)], with dimensions of length. Note that the basis waves $W_{\{r,l\}}(x)$ are eigenfunctions of the projection operators with eigenvalues of either 0 or 1.

Given a solution $\bar{P}(x)$ for the pressure obtained in the presence of mechanical perturbations, the projection operators $\hat{P}_{\{r,l\}}$ enable one to find the forward- and reverse-traveling wave components at any point in the cochlea. In particular, one can use them to determine the cochlear reflectance, defined by Eq. (13). Although the solution $\bar{P}(x)$ can, of course, be obtained numerically, the analytic expression derived in the next section provides crucial insight.

B. Finding the pressure in the presence of perturbations

1. Response to a point source on the BM

We solve the scattering problem by first supposing that we have solved a simpler problem: finding the response in an otherwise smooth cochlea to an isolated point source on the BM. We therefore define the complex-valued 2-D Green's function $G(x,y|x',y')$ as the solution to Poisson's equation,

$$(\partial_x^2+\partial_y^2)G=-\delta(x-x')\,\delta(y-y'), \tag{26}$$

where $\delta(x)$ is the Dirac delta function. Since the product of delta functions vanishes identically except at the point (x',y'), the right-hand side represents an oscillating point source of unit strength located at position (x',y'). The dimensionless Green's function $G(x,y|x',y')$ describes the propagated response at the observation point (x,y) to the source at (x',y') and is understood to satisfy the boundary conditions imposed on the pressure in the cochlea. For example, $G(x,y|x',y')$ depends on the BM impedance via the frequency-dependent boundary condition $\partial_y \ln G=HZ_{\mathrm{f}}/Z_{\mathrm{BM}}$ along the BM [Eq. (11) for a smooth cochlea]. The Green's function is symmetric (reciprocal) under the interchange of source and observation points within the cochlea: $G(x,y|x',y')=G(x',y'|x,y)$. In other words, the response at (x,y) to a source at (x',y') is identical to the response at (x',y') to the same source at (x,y). In our application we take $y'=0^+$ since the sources (perturbations) are presumed to be located on the BM (i.e., at $y=0^+$) rather than somewhere off in the fluid $(y>0)$.

2. An integral equation for the pressure

We now use the Green's function $G(x,y|x',y')$ to obtain an integral representation for the pressure $P(x,y)$. We start with the identity

$$P(x,y)=\frac{1}{b}\iint_{S'} G(x,y|x',y')\partial_{\perp'}P(x',y') - P(x',y')\partial_{\perp'}G(x,y|x',y')dS', \quad (27)$$

where S' is the total boundary surface of the scala vestibuli and $\partial_\perp \equiv (\mathbf{e}_\perp \cdot \nabla)$ represents the derivative in the direction of the local outward normal to the surface (e.g., $\partial_{\perp'} = -\partial_{y'}$ along the BM). Equation (27) is obtained by integrating $G\nabla^2 P - P\nabla^2 G$ over the scala volume and converting the result into a surface integral over S' using Green's theorem (e.g., Courant, 1988).

To evaluate the contributions from the various boundary surfaces we assume that the pressure $P(x',y')$ results from a stimulus applied at the stapes. In the absence of mechanical perturbations, $P(x',y')$ is simply the unperturbed pressure distribution, which we take equal to the forward-traveling wave, $P_r(x',y')$. We now assume, however, that $P(x,y)$ contains effects arising from roughness; near the stapes we therefore expect $P(x',y')$ to comprise both forward- and reverse-traveling wave components. The boundary conditions on $G(x,y|x',y')$ and $P(x',y')$ discussed in Sec. II imply that the only nonzero contributions to the surface integral arise from the basal boundary at the stapes ($x'=0$) and from the lower boundary at the BM ($y'=0^+$). Evaluating these terms yields the integral equation

$$P(x,y)=P_r(x,y)+H\int_0^\infty G(x,y|x',0^+) \times \epsilon(x')k_{\mathrm{lw}}^2(x')P_0(x')dx'. \quad (28)$$

To obtain Eq. (28) we used the fact that along the BM $\partial_{y'}\ln P_0 = HZ_{\mathrm{f}}/\tilde{Z}_{\mathrm{BM}} = (1+\epsilon)Hk_{\mathrm{lw}}^2$ [Eqs. (11), (17), and (21)]; the Green's function $G(x,y|x',0^+)$ is defined in the smooth cochlea and therefore satisfies the same boundary condition with $\epsilon=0$. Note that Eq. (28) for $P(x,y)$ reduces to the unperturbed right-going solution, $P_r(x,y)$, in the absence of roughness.

To obtain an integral equation for the pressure $\bar{P}(x)$ we average Eq. (28) over the scala cross section:

$$\bar{P}(x)=\bar{P}_r(x)+\int_0^\infty \bar{G}_0(x|x')\varrho(x')\bar{P}(x')dx', \quad (29)$$

where $\varrho \equiv \epsilon k^2 \equiv \epsilon\alpha k_{\mathrm{lw}}^2$ and

$$\bar{G}_0(x|x') \equiv \int_0^H G(x,y|x',0^+)dy. \quad (30)$$

The function $\bar{G}_0(x|x')$ has units of length and describes the propagated response, averaged over the duct cross section at the observation point at x, to the BM source at x'. Equation (29) therefore represents the mechanical perturbations as a distribution of BM point sources with strengths that vary with position, x'. At any point x, the scalae-averaged pressure resulting from the distribution of sources is found by adding up the response to each source, $\bar{G}_0(x|x')$, weighted by the corresponding source strength, $\varrho\bar{P}$. In the continuum limit, the summation becomes an integral over the source distribution, where the integration extends over all regions of the cochlea where ϱ is nonzero.

Although the function $\bar{G}_0(x|x')$ defined by Eq. (30) plays a role in Eq. (29) analogous to a one-dimensional Green's function, $\bar{G}_0(x|x')$ is not a conventional Green's function. Note, for example, that $\bar{G}_0(x|x')$ is not symmetric under the interchange of source (x') and observation (x) points within the cochlea. This lack of symmetry is no violation of reciprocity; it simply reflects the basic asymmetry between source and observation inherent in the definition of $\bar{G}_0(x|x')$: Whereas the source occurs on the BM [i.e., at the point $(x',0^+)$] the observation comprises a vertical average over the scalae cross section [i.e., $(x,\int dy)$]. To avoid confusion we refer to $\bar{G}_0(x|x')$ as the "reduced traveling-wave Green's function."

3. An iterative solution

Although Eq. (29) for $\bar{P}(x)$ is purely formal—the first term is known but the unknown solution $\bar{P}(x)$ appears inside the integral—we can construct an explicit solution $\bar{P}(x)$ by iteration. Making the notational substitutions $x'\to x''$ and $x\to x'$ in Eq. (29) yields

$$\bar{P}(x')=\bar{P}_0 W_r(x')+\int \bar{G}_0(x'|x'')\varrho(x'')\bar{P}(x'')dx'', \quad (31)$$

where $\bar{P}_0 \equiv \bar{P}_r(0)$. Inserting this expression for $\bar{P}(x')$ into the integral on the right-hand side of Eq. (29) yields

$$\bar{P}(x)=\bar{P}_0 W_r(x)+\bar{P}_0\int dx'\bar{G}_0(x|x')\varrho(x')W_r(x') + \int dx'\bar{G}_0(x|x')\varrho(x') \times \int dx''\bar{G}_0(x'|x'')\varrho(x'')\bar{P}(x''). \quad (32)$$

The first two terms on the right-hand side of this equation are now known; the unknown function $\bar{P}(x)$ appears only in the third.

By iterating in this fashion we construct the cochlear "Born expansion."[5] Each iteration introduces another power of the perturbations, ϱ. If the perturbations are weak, each additional term is smaller than the one preceding it. Successive iterations then push the unknown function $\bar{P}(x)$ into smaller and smaller terms. Eventually the contribution from this unknown function can be neglected and the solution expressed entirely in terms of known quantities. More formally, let $\bar{P}_1(x) \equiv \bar{P}_0 W_r(x)$ and

$$\bar{P}_{n+1}(x) \equiv \int \bar{G}_0(x|x')\varrho(x')\bar{P}_n(x')dx', \quad (33)$$

for $n=1,2,3,\ldots$. If the series converges, the solution to the integral equation is

$$\bar{P}(x)=\sum_{n=1}^{\infty}\bar{P}_n(x). \tag{34}$$

4. Interpretation as multiple scattering

Series (34) can be interpreted physically as arising from multiple scattering. Each term $\bar{P}_n(x)$ represents the contribution of wavelets scattered $n-1$ times within the cochlea (n is the number of intervals of scatter-free propagation). For example, the term $\bar{P}_3(x)$, defined by the double integral

$$\bar{P}_3(x)=\bar{P}_0\int dx'\,\bar{G}_0(x|x')\varrho(x')\times\int dx''\bar{G}_0(x'|x'')\varrho(x'')W_r(x''), \tag{35}$$

represents the net contribution of all doubly scattered wavelets. The wavelets contributing to $\bar{P}_3$ first propagate freely to x'', where they scatter with strength $\varrho(x'')$. The scattered wavelets then propagate freely to x', where they scatter a second time with strength $\varrho(x')$ before propagating a third and final time to the observation point at x. Since x'' and x' can be located anywhere in the cochlea—in particular, x' can be either apical to or basal to x''—both forward and backward scattering are properly accounted for. The integration over the coordinates x'' and x' thus sums contributions from all pairwise combinations of scattering locations within the cochlea. Finally, summing the terms $\bar{P}_n(x)$ combines wavelets scattered all possible number of times.

C. Approximate form of the reduced traveling-wave Green's function

Practical application of scattering series (34) for $\bar{P}(x)$ requires knowledge of the reduced Green's function, $\bar{G}_0(x|x')$. Ideally one seeks an expression for $\bar{G}_0(x|x')$ valid throughout the cochlea, but to understand the effect of perturbations on the reflectance evaluated at the stapes it suffices to find an approximation valid in the "far field" at some distance from the source at x'. To obtain an approximate form for $\bar{G}_0(x|x')$ valid in this regime we begin by writing $G(x,y|x',y')$ in the form

$$G(x,y|x',y')=G(x|x')Q(y;x|y';x'), \tag{36}$$

where $G(x|x')$ is the traveling-wave Green's function for the equivalent long-wave model (i.e., the long-wave model with the same basis waves) and $Q(y;x|y';x')$ remains undetermined. $G(x|x')$ is defined as the symmetric solution to

$$(\partial_x^2+k^2)G(x|x')=-\delta(x-x'), \tag{37}$$

subject to the appropriate boundary conditions at the base and apex of the cochlea. By writing $G(x,y|x',y')$ in the product form (36) we "factor out" the principal traveling-wave solutions that couple to the stapes. The undetermined function $Q(y;x|y';x')$ thus provides the residual y (and x) dependence. $Q(y;x|y';x')$ has units of reciprocal length and is normalized so that

$$\frac{1}{H}\int_0^H dy\int_0^H dy'\,Q(y;x|y';x')\cong 1. \tag{38}$$

The normalization is exact in the long-wave regime and approximate elsewhere; it guarantees that $G(x,y|x',y')$ reduces to $G(x|x')$ in the limit that the source distribution at x' is independent of y' and the response at x is averaged over y. In the long-wave limit, pressures—and pressure sources—are uniform over the scalae.

According to definition (30), $\bar{G}_0(x|x')$ has the value

$$\bar{G}_0(x|x')=G(x|x')\int_0^H Q(y;x|0^+;x')dy. \tag{39}$$

To obtain an approximate expression for the integrand $Q(y;x|0^+;x')$ we argue physically as follows: When the cochlea is driven from the stapes, the pressure $P_0(x)$ at the BM is $\alpha(x)$ times the "line-averaged" pressure $\bar{P}(x)$ in the fluids above [i.e., $P_0(x)=\alpha(x)\bar{P}(x)$, by Eq. (18)]. In an analogous way, when the driving source at x' is located on the BM ($y=0^+$), we expect the far-field component of the response to be $\alpha(x')$ times the response to a "line source" of equivalent total strength spread out uniformly over the interval $(0,H)$. In other words, we expect that

$$Q(y;x|0^+;x')\cong\alpha(x')\frac{1}{H}\int_0^H Q(y;x|y';x')dy'. \tag{40}$$

Substituting this value into Eq. (39) and applying the normalization (38) yields the approximation

$$\bar{G}_0(x|x')\cong\alpha(x')G(x|x'). \tag{41}$$

We derive a general expression for the 1-D traveling-wave Green's function, $G(x|x')$, in Appendix B. The expression for $G(x|x')$ [Eq. (B8)] is symmetric in x and x' and includes the effect of nonzero reflection from the stapes. Since our goal here is to calculate the cochlear reflectance, a quantity independent of the stapes boundary condition, we assume for simplicity that the stapes presents a perfectly reflectionless boundary ($R_{\text{stapes}}=0$). In this case, the long-wave Green's function $G(x|x')$ reduces to $G_\infty(x|x')$, where the subscript indicates that the cochlea appears infinite in extent to waves incident upon the stapes. According to Appendix B, $G_\infty(x|x')$ is given by

$$G_\infty(x|x')=\gamma W_l(x_<)W_r(x_>), \tag{42}$$

where $x_<(x,x')\equiv\min(x,x')$ and $x_>(x,x')\equiv\max(x,x')$. Derived here on physical grounds, approximation (41) is proved formally in Appendix C for the case when the BM impedance is independent of position; the proof generalizes to yield an approximate expression valid when the smooth component of the BM impedance varies slowly with x.

Figure 6 compares approximation (41) to the "exact" Green's function $\bar{G}_0(x|x')$ computed numerically. As expected, systematic deviations between the two solutions appear when both source and observation points (x and x') are close to the characteristic place (i.e., in the short-wave "near field"). Nevertheless, the approximation is uniformly excellent in the far-field regime ($x\to 0$) relevant here.

D. First-order approximation for the reflectance

Equation (34) constructs the solution $\bar{P}(x)$ in the form of a perturbative "scattering series." When the perturbations

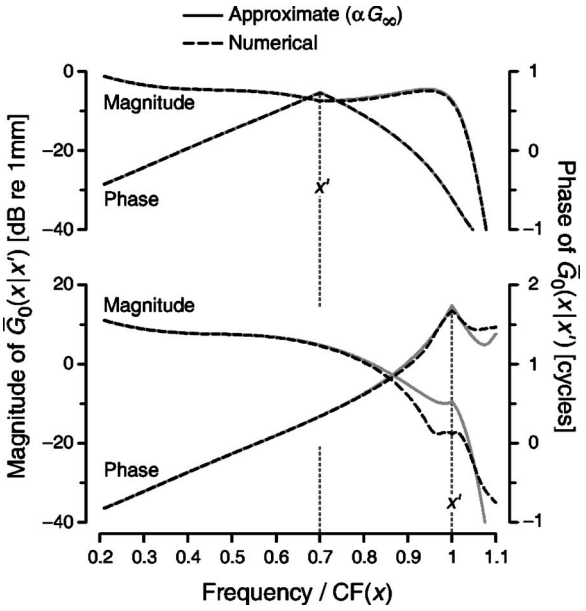

FIG. 6. Reduced traveling-wave Green's functions $\bar{G}_0(x|x')$ for two source locations x'. The observation point x varies along the abscissa and is shown in the form $f/\mathrm{CF}(x)$, where f is the source frequency. When the model is driven from the stapes, the peak of the corresponding BM velocity response occurs at the value 1. Magnitude and phase scales are shown on the left- and right-hand sides of the plot, respectively. Vertical dotted lines mark the two source locations x'. The top panel shows $\bar{G}_0(x|x')$ for an off-peak source located at a point whose CF is more than half an octave above the source frequency $[f/\mathrm{CF}(x')=0.7]$. The bottom panel shows $\bar{G}_0(x|x')$ for a source located at the characteristic place $[f/\mathrm{CF}(x')=1]$. The stapes was assumed perfectly transparent ($R_{\mathrm{stapes}}=0$). The dashed lines show the "exact" Green's functions computed numerically (standard model parameters from Appendix D); the solid lines show the approximate Green's function derived in the text [$\bar{G}_0\cong\alpha G_\infty$, Eqs. (41) and (42)]. The approximation is uniformly excellent as $x\to 0$ and breaks down only when both x and x' are in the short-wave regime close to the characteristic place.

are small one can neglect secondary ($n>2$) scattering by truncating series (34) after the first two terms ($\bar{P}_1+\bar{P}_2$). One then obtains an expression for $\bar{P}(x)$ valid to first order in ϱ (the so-called Born approximation):

$$\bar{P}(x)\cong\bar{P}_0 W_r(x)+\bar{P}_0\int \bar{G}_0(x|x')\varrho(x')W_r(x')dx'. \tag{43}$$

Substitution of the explicit form for $\bar{G}_0(x|x')$ [Eqs. (41) and (42)] yields the approximation

$$\bar{P}(x)\cong\bar{P}_0\left[1+\gamma\int_0^x \varrho\,\alpha W_l W_r\,dx'\right]W_r(x) + \bar{P}_0\left[\gamma\int_x^\infty \varrho\,\alpha W_r^2\,dx'\right]W_l(x). \tag{44}$$

We take the integration to ∞ in the final term as a reminder that we have assumed the cochlea is essentially infinite in extent (i.e., no wave reflection occurs at the helicotrema). In practice, the magnitude of the integrand rapidly falls to zero apical to the peak of the traveling wave; at all but the lowest frequencies the precise value of the upper limit is therefore irrelevant.

The two terms in brackets describe how nonzero perturbations ϱ cause the forward- and reverse-traveling wave amplitudes to vary with position. The cochlear reflectance (13) can be found as the ratio at $x=0$ of the coefficients of $W_l(x)$ and $W_r(x)$ in the series representation of $\bar{P}(x)$. These coefficients can be read off directly from Eq. (44) or, in the more general case, computed by using the projection operators $\hat{P}_{\{r,l\}}$ [Eq. (25)]. To first order in ϱ,

$$R\cong R_{\mathrm{Born}}\equiv\gamma\int_0^\infty \varrho\,\alpha W_r^2\,dx=\gamma\int_0^\infty \epsilon\alpha k^2 W_r^2\,dx. \tag{45}$$

Higher-order approximations to the reflectance that include the effects of multiple scattering are easily derived using series (34). When the various factors in the integrand are replaced by their long-wave equivalents (i.e., $\alpha\to 1$; $k^2\to k_{\mathrm{lw}}^2$; and $W_r^2\to W_{\mathrm{lw},r}^2$), approximation (45) for R reduces to the expression previously derived for the 1-D model (Shera and Zweig, 1993b; Zweig and Shera, 1995; Talmadge *et al.*, 1998).[6]

V. CONTROLLING FOR VARIATIONS IN MECHANICAL TUNING

Before applying our perturbative expression for the cochlear reflectance [Eq. (45)], we need to eliminate spurious sources of variation. Recall that our goal is to understand how the character of the wave scattering in the peak region (i.e., long-wave versus short-wave) modifies the predictions of the theory. We approach the problem via a thought-experiment. Imagine a family of models whose parameters (specifically, the scalae height H and partition impedance function Z_{BM}) differ in ways that yield different values of $\hat{k}H$. In order not to confound our analysis of long- and short-wave scattering, we need to restrict attention to those parameter sets that yield realistic mechanical tuning. In particular, we demand that the BM velocity response for the smooth cochlea, $V_{\mathrm{BM}}(x)$, be held fixed at some predetermined value. Unless $V_{\mathrm{BM}}(x)$ is held fixed, variations in the reflectance that result from changes in mechanical tuning may be mistakenly ascribed to differences between short- and long-wave scattering. Our question thus becomes: How does the reflectance R vary among models of different heights or dimensionality constructed so that they reproduce the same BM velocity response but manifest different values of $\hat{k}H$?

To address this question we must determine how to enforce the constraint of constant tuning. In a nutshell, the problem is to find 1-D and 2-D models that reproduce a given BM velocity response. In other words, we need to solve the cochlear inverse problem. Unfortunately, existing methods (e.g., Zweig, 1991; de Boer, 1995a,b; de Boer and Nuttall, 1999) do not serve our application, and we therefore develop an alternative approach.

A. Finding the wave number from the BM velocity

We first demonstrate that fixing $V_{\mathrm{BM}}(x)$ is equivalent to fixing the wave number, $k(x)$, that appears in the one-dimensional wave equation for $\bar{P}$ [Eq. (19)]. This result makes intuitive sense—since $V_{\mathrm{BM}}(x)$ is the traveling wave, fixing its value necessarily fixes its various properties, among them its wave number, $k(x)$.

We begin by writing Eq. (10) for Z_{BM} in the form

$$P_0 = bZ_{\mathrm{BM}}V_{\mathrm{BM}}. \tag{46}$$

Multiplying both sides by k^2/α and simplifying [using Eqs. (17), (18), and (20)] allows us to rewrite this equation in terms of $\bar{P}$ and k rather than P_0 and Z_{BM}. The result is

$$k^2\bar{P} = -bZ_{\mathrm{f}}V_{\mathrm{BM}}. \tag{47}$$

If we then substitute this expression for $k^2\bar{P}$ into wave equation (22), we obtain an equation for $\bar{P}(x)$ in which the unknown wave number $k(x)$ does not appear:

$$\partial_x^2\bar{P} = bZ_{\mathrm{f}}V_{\mathrm{BM}}. \tag{48}$$

Now, if the function $V_{\mathrm{BM}}(x)$ is known—whether by model or by measurement—Eq. (48) can be solved for $\bar{P}$ by double integration:

$$\bar{P}(x) = bZ_{\mathrm{f}}\int_x^L dx' \int_{x'}^L V_{\mathrm{BM}}(x'')dx''. \tag{49}$$

The constants of integration are chosen to satisfy the boundary conditions (in this case, $\bar{P} = \partial_x\bar{P} = 0$ at the helicotrema). Using our solution (49) for $\bar{P}(x)$ we can then determine the wave number using Eq. (47):

$$k^2(x) = -V_{\mathrm{BM}}(x) \Big/ \int_x^L dx' \int_{x'}^L V_{\mathrm{BM}}(x'')dx''. \tag{50}$$

Thus, the wave number $k(x)$ depends only on the given BM response function, $V_{\mathrm{BM}}(x)$, and is independent of the value of H, the effective height of the model. In other words, fixing $V_{\mathrm{BM}}(x)$ yields the same wave number irrespective of whether the model is everywhere long wave, or short wave, or manifests a transition between the two, as in the real cochlea.

Note that Eq. (50) determines $k(x)$ not by assuming a particular form for $Z_{\mathrm{BM}}(x)$, but by requiring that the model match a given BM-velocity response, $V_{\mathrm{BM}}(x)$. In other words, Eq. (50) provides a partial solution to the inverse problem (partial because it determines k^2 but not Z_{BM}). The wave number inversion procedure derived here is a two-dimensional variant of the procedure suggested by de Boer (1995a). An alternative procedure, analogous to Zweig's (1991) iterative long-wave method, can be developed based on approximate WKB solutions for $\bar{P}(x)$.

B. Finding the partition impedance from the wave number

Controlling for changes in mechanical tuning that would otherwise occur when we vary the height of the model requires varying the model parameters so that the wave number remains independent of H. To accomplish this, and thereby provide a full solution to the inverse problem, we must determine the corresponding BM impedance. Note that our analysis implies that constant mechanical tuning can only be maintained across models of different heights if the BM impedance varies with H. This conclusion should come as no surprise—it merely inverts the more familiar result that $V_{\mathrm{BM}}(x)$ depends on the assumed height of the model when $Z_{\mathrm{BM}}(x)$ is (tacitly) held constant.

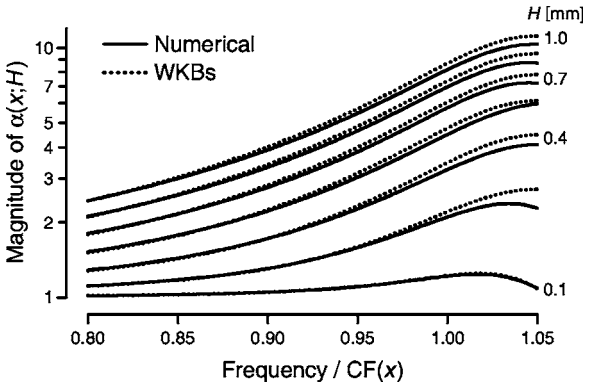

FIG. 7. Magnitude of $\alpha(x;H)$ for various values of H. The figure shows $|\alpha(x;H)|$ near the peak of the BM velocity response, located at the value 1 along the abscissa. Magnitudes are shown at seven equally spaced values of H spanning the interval [0.1,1] mm. Solid lines show $\alpha(x;H)$ computed numerically; dotted lines show the approximate WKB expression $\alpha_{\mathrm{WKBs}}(x;H)$ from Eq. (52). The BM velocity response, $V_{\mathrm{BM}}(x)$, was held fixed using the standard model parameters (Appendix D).

More significantly, the analysis indicates *how* $Z_{\mathrm{BM}}(x)$ must vary with H to maintain constant tuning. According to Eq. (20) the BM impedance and wave number are related by the equation

$$k^2(x) = -\alpha(x)Z_{\mathrm{f}}/Z_{\mathrm{BM}}(x). \tag{51}$$

Equation (51) implies that the ratio $\alpha(x)Z_{\mathrm{f}}/Z_{\mathrm{BM}}(x)$ must be independent of H if $V_{\mathrm{BM}}(x)$ and $k^2(x)$ are to remain invariant. In other words, $Z_{\mathrm{BM}}(x;H)$ must vary with H in exactly the same way as $\alpha(x;H)Z_{\mathrm{f}}$ so that the H dependence cancels in the ratio.

Figure 7 shows how $\alpha(x;H)$ varies with H at fixed $k(x)$. In the process, we compare numerical results with the approximation $\alpha_{\mathrm{WKBs}}(x;H)$ computed from the standard WKB expression for $P(x,y)$ (e.g., Steele and Taber, 1979; Viergever, 1980; de Boer and Viergever, 1982), which yields[7]

$$\alpha(x;H) \cong \alpha_{\mathrm{WKBs}}(x;H) = \frac{k(x)H}{\tanh[k(x)H]}. \tag{52}$$

Although the approximation is generally a good one, systematic deviations are apparent near the peak of the traveling wave. Note that the WKB formula implies that $\alpha(x;H) \cong \alpha[k(x)H]$, a result that makes sense on dimensional grounds: Since $\alpha(x)$ is a dimensionless ratio, it can only be a function of dimensionless products, and the wave number k is the natural quantity with units of inverse length needed to cancel the units of H.

Equation (51)—together with the good but imperfect approximation $\alpha(x) \cong \alpha_{\mathrm{WKBs}}(x)$ illustrated in Fig. 7—suggests an iterative inversion procedure for finding the functions $\alpha(x)$ and $Z_{\mathrm{BM}}(x)$ needed to evaluate Eq. (45) for R and/or to solve the model numerically under the constraint of constant tuning. Figure 8 illustrates the procedure, which begins by using Eq. (50) to find the wave number, $k(x)$, corresponding to the target BM velocity response function, $V_{\mathrm{BM}}(x)$. Then, after using the WKB approximation to provide initial estimates of $\alpha(x)$ and $Z_{\mathrm{BM}}(x)$, the algorithm iteratively improves these estimates, ultimately converging on a self-

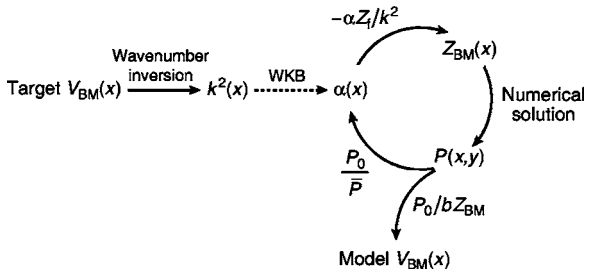

FIG. 8. Iterative inverse method for finding and solving the 2-D model equations that yield a target BM velocity response. The algorithm begins on the left, outside the loop. First, the target $V_{BM}(x)$ is used to determine the corresponding wave number, $k^2(x)$ [Eq. (50)]. An initial estimate of $\alpha(x)$ is then calculated (dotted line) using the standard WKB approximation [Eq. (52)]. Upon entering the loop, the approximate $\alpha(x)$ is used to estimate the corresponding BM impedance, $Z_{BM}(x)$ [Eq. (51)]. Numerical solution of Laplace's equation, with $Z_{BM}(x)$ defining the BM boundary condition, yields the pressure field $P(x,y)$, from which $\bar{P}(x)$, $P_0(x)$, and an improved estimate of $\alpha(x)$ are determined [Eqs. (14), (16), and (18)]. The loop then begins anew, using the improved estimate of $\alpha(x)$ to compute the BM impedance. Iteration continues until the algorithm converges on mutually consistent solutions for $\alpha(x)$, $Z_{BM}(x)$, and $P(x,y)$. The model's BM velocity response [Eq. (46)] then matches the target value.

consistent solution that reproduces the given velocity response. [In practice, no more than two to three iterations are needed to achieve good convergence. If too many iterations are employed, the solution can begin to diverge again just beyond $\hat{x}$. We believe that this instability arises from nonpropagating pressure modes that somehow slink into the solution from their usual innocuous hangout in the cutoff region apical to the characteristic place (e.g., de Boer and Viergever, 1982; Watts, 2000).] Although the initial WKB estimate for $\alpha(x)$ is often a good one (cf. Fig. 7), relatively small changes in $\alpha(x)$ can produce large changes in $V_{BM}(x)$ via their effect on the BM impedance in the region of traveling-wave amplification ($\mathrm{Re}\{Z_{BM}\}<0$) just basal to the peak (see Sec. VII C). The iterative procedure therefore generally improves the overall quality of the solution substantially.

C. The inverse procedure in action

Figure 9 illustrates the application of our inversion procedure. The bottom panel shows two BM impedance functions [$Z^{1d}_{BM}(x)$, dashed line; and $Z^{2d}_{BM}(x)$, solid line] that yield identical velocity responses (top panel) when employed in 1-D and 2-D models, respectively (standard model parameters from Appendix D). We refer to models of different heights or dimensionality that yield the same $V_{BM}(x)$ as "response-matched models." In this case, the target BM velocity response and the impedance Z^{1d}_{BM} were obtained using a variant of the long-wave model of Zweig (1991) as described in Appendix D; Z^{2d}_{BM} was computed using the inverse method diagrammed in Fig. 8.

Although Z^{1d}_{BM} and Z^{2d}_{BM} share a common qualitative form, including a bowl-shaped region of negative resistance in the region basal to the traveling-wave peak,[8] they also manifest important quantitative differences. Since $k^2(x)$ is invariant, Eq. (51) implies that

$$Z^{2d}_{BM}(x)=\alpha(x)Z^{1d}_{BM}(x). \tag{53}$$

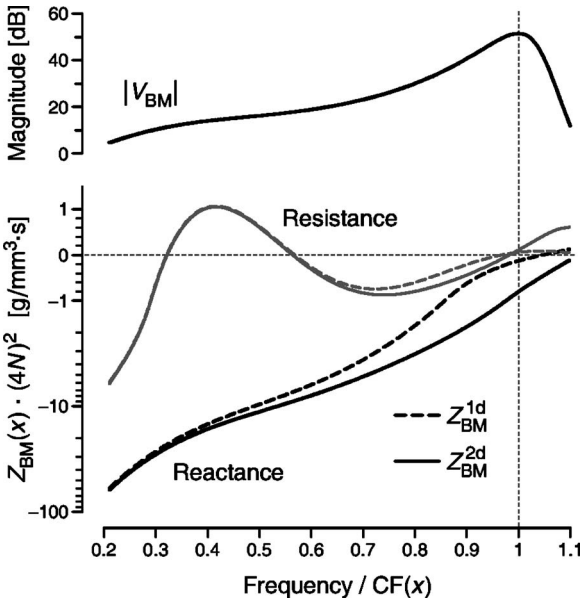

FIG. 9. BM impedance functions (bottom panel) that yield identical mechanical tuning (top panel) in 1-D and 2-D models. The real and imaginary parts of the 2-D impedance, $Z^{2d}_{BM}(x)$ (bottom panel, solid lines), were computed using the inverse procedure outlined in Fig. 8 with a target BM velocity response (magnitude shown in top panel) obtained from a variant of the long-wave model of Zweig (1991) (see Appendix D). The impedance of the 1-D model, $Z^{1d}_{BM}(x)$, is shown with dashed lines. The y-axis scale has been warped to accommodate the wide range of positive and negative impedance values (see Shera *et al.*, 2000, footnote 17); the scale is linear on the interval $[-1,1]$ and logarithmic elsewhere. For reference, a horizontal dotted line intersects the impedance ordinate at 0 and a vertical dotted line locates the peak of the target BM velocity response along the abscissa. The function $\alpha(x)$ corresponding to $Z^{2d}_{BM}(x)$ is shown in Fig. 5 ($\alpha=1$ in the 1-D model).

As expected from the form of $\alpha(x)$ (shown for the same model parameters in Fig. 5), $Z^{1d}_{BM}(x)$ and $Z^{2d}_{BM}(x)$ are essentially indistinguishable in the long-wave region near the stapes but gradually diverge from one another as the traveling wave in the 2-D model enters the short-wave regime. Basal to the characteristic place, $\alpha(x)$ is approximately real and the two impedances therefore differ mostly by a position-dependent scale factor, with $|Z^{2d}_{BM}|>|Z^{1d}_{BM}|$. Just apical to $\hat{x}$, however, the phase of $\alpha(x)$ begins to change rapidly; as a result the relative magnitudes of the resistive and reactive components of the two impedances change. Note, for example, that although $\hat{x}$ is invariant (by design), the "resonant place" of the partition in the 2-D model (as defined by the zero-crossing of the reactance) occurs at a location considerably apical to its 1-D counterpart. (Equivalently, scaling implies that the local "resonant frequency" in the 2-D model appears shifted to higher frequencies.) Thus, the short-wave hydrodynamics in the 2-D model exaggerate an effect already apparent in 1-D: The CF at location x occurs at a frequency well above the *in vacuo* resonant frequency of the partition; in active models (both 1-D and 2-D) the best place is determined more by the zero crossing of the resistance than by the zero crossing of the reactance.

VI. SHORT-WAVE AND LONG-WAVE SCATTERING

Now that we are able to eliminate spurious variations in mechanical tuning, we return to our central question. Figure

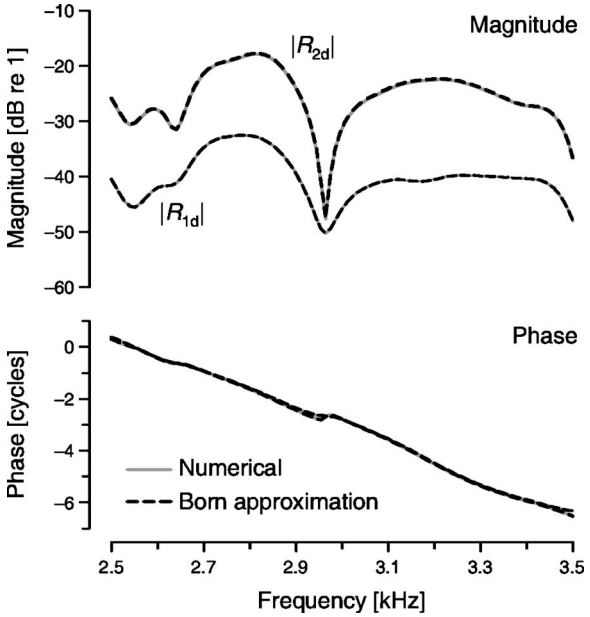

FIG. 10. Cochlear reflectances R_{1d} and R_{2d} versus frequency. The top and bottom panels show reflectance magnitudes and phases as computed in response-matched 1-D and 2-D models [$V_{BM}(x)$ held constant] using identical random impedance perturbations of magnitude $|\epsilon| \sim \mathcal{O}(1/100)$. Nonperturbative numerical calculations are shown with gray solid lines; the first-order Born approximation from Eq. (45) is shown with dashed lines. Standard model parameters are given in Appendix D.

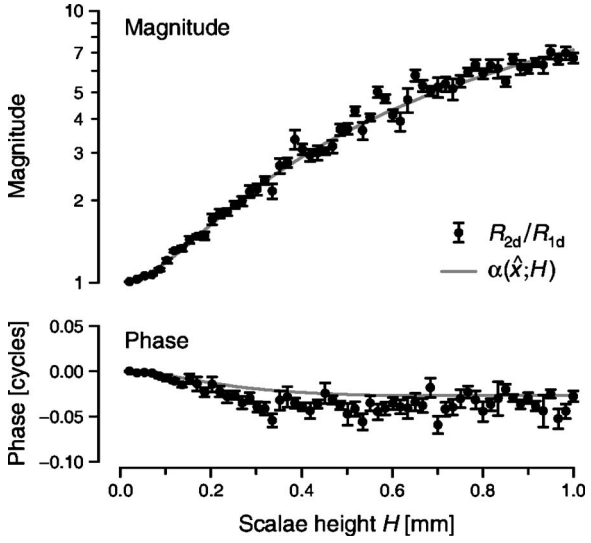

FIG. 11. Reflectance ratio R_{2d}/R_{1d} versus scalae height, H. Data points and error bars represent means and standard deviations of 20 ratios calculated from paired values of R_{1d} and R_{2d} computed numerically in response-matched 1-D and 2-D cochlear models at fixed frequency. Each of the 20 pairs of 1-D and 2-D simulations represented by every point employed a different random realization of the impedance perturbations, $\epsilon(x)$. Ratios were computed at 60 scalae heights spanning the range [0.02,1] mm. The approximation $R_{2d}/R_{1d} \cong \alpha(\hat{x};H)$ from Eq. (55) is shown for comparison (gray line).

10 compares the reflectances R_{1d} and R_{2d} computed in 1-D and 2-D models constructed to have the same BM velocity response (i.e., response-matched models). Identical random impedance perturbations (with $|\epsilon| \sim 1\%$) were used in each case. The reflectances R_{1d} and R_{2d} both share features characteristic of measured stimulus-frequency and transient-evoked OAEs, including a rapidly rotating phase and an amplitude spectrum whose leisurely noodling about is occasionally punctuated by deep notches (reviewed in Shera and Guinan, 1999). Although their phase versus frequency functions are very similar, R_{1d} and R_{2d} differ substantially in overall magnitude, with $|R_{2d}| \gg |R_{1d}|$ for the standard parameters used here. The figure also demonstrates that the first-order perturbative expression for R given in Eq. (45) closely matches the nonperturbative numerical calculation. Our analytic expression for R_{Born} therefore allows us to probe the origin of the differences between R_{1d} and R_{2d}.

A. Relation between 1-D and 2-D reflectances

Figure 11 plots the complex reflectance ratio R_{2d}/R_{1d} as a function of H at fixed frequency. Each data point and its error bar represents the mean and standard deviation of 20 ratios computed from numerical computations of R_{1d} and R_{2d} in response-matched 1-D and 2-D cochlear models of varying height [$V_{BM}(x)$ held constant].[9] Every pair of simulations employed a different random realization of the impedance perturbations, $\epsilon(x)$. As a gross consistency check on the calculations note that $\lim_{H \to 0} R_{2d}/R_{1d} = 1$, as expected. Although the simulations show a small systematic shift in the reflectance phase, the largest effect of the short-wave hydrodynamics is the substantial increase in reflectance magnitude evident at larger values of H.

To understand these results, recall that Eq. (45) for R_{Born} reads

$$R_{Born} = \gamma \int_0^\infty \epsilon \alpha k^2 W_r^2 \, dx. \tag{54}$$

We begin the analysis by asking how the factors in the integrand (i.e., ϵ, α, k^2, and W_r^2) depend on H when $k(x)$ is held fixed. Since we are considering the physically reasonable case where the fractional size of the perturbations ($\Delta Z_{BM}/Z_{BM}$) remains constant, ϵ is independent of H by hypothesis. The factor of k^2 is also clearly independent of H at fixed k, and we have already determined that $\alpha(x;H) \cong \alpha[k(x)H]$ varies with H [see Fig. 7 and Eq. (52)]. What about the factor W_r^2? Since the basis waves $W_{\{r,l\}}(x)$ are solutions of the equation $(\partial_x^2 + k^2) W_{\{r,l\}} = 0$ in which H does not explicitly appear, the basis waves (and the value of γ derived from them) depend only on $k(x)$; consequently, when $k(x)$ is fixed, so too are the basis waves $W_{\{r,l\}}(x)$. We conclude, then, that when $V_{BM}(x)$ is held constant, $\alpha(x;H)$ is the only factor contributing to the reflectance that varies with H. Differences between short- and long-wave scattering thus originate entirely in the function $\alpha(x;H)$.

Roughly speaking, the hydrodynamics encapsulated by $\alpha(x;H)$ can be thought of as modifying the effective strength of the perturbations. For example, Eq. (54) reduces to the 1-D result if the effective perturbations in the 1-D model are taken to be $\epsilon_{eff}(x;H) = \alpha(x;H)\epsilon(x)$. Since $|\alpha| > 1$, the short-wave hydrodynamics act, in effect, to magnify the perturbations, and we therefore expect $|R_{2d}| > |R_{1d}|$, consistent with the results in Figs. 10 and 11. As demonstrated below, the dominant scattering occurs in a region straddling the peak of the integrand, which is generally located close to the characteristic place. [The location of the peak of the integrand is

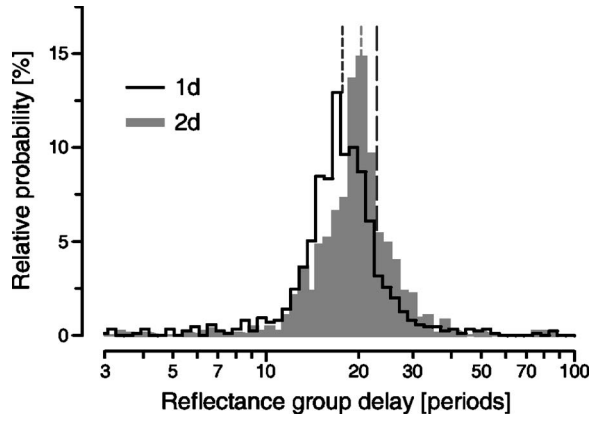

FIG. 12. Reflectance group delays in response-matched 1-D and 2-D models. The figure shows histograms of reflectance group delays (in periods of the stimulus frequency) pooled from 50 simulations, each employing a different random distribution of mechanical perturbations. In each simulation, the stimulus frequency was varied over a small neighborhood about 3 kHz (± 80 Hz in 10-Hz steps), and reflectance group delays (defined as $\tau \equiv -\partial_\omega \angle R$) were found by computing local phase gradients from unwrapped phase responses using centered differences (Shera and Guinan, 2003). The two short-dashed vertical lines that intersect the histogram peaks indicate group delays estimated from the phase gradient of the smooth component of the integrand in Eq. (54), evaluated at its magnitude peak [Eq. (57)]. The long-dashed line on the right shows twice the CF group delay of the corresponding BM velocity transfer function.

somewhat variable because the perturbations $\epsilon(x)$ vary "randomly" from cochlea to cochlea.] To the extent that $\alpha(x;H)$ is roughly constant over the scattering region it can be pulled outside the integral, yielding the approximate relation

$$R_{2\mathrm{d}} \cong \alpha(\hat{x};H)\,\gamma \int_0^\infty \epsilon k^2 W_r^2\, dx \cong \alpha(\hat{x};H) R_{1\mathrm{d}}. \tag{55}$$

In the short-wave region the magnification factor thus has the approximate value $\alpha(\hat{x};H) \cong \hat{k}H$. (Estimated values of $\hat{k}H$ are shown for human and guinea pig cochleae in Fig. 1.) The accuracy of approximation (55) in any given cochlea (or cochlear model) depends on the precise distribution of impedance perturbations. At best, its validity is therefore only statistical. To test Eq. (55), Fig. 11 also plots the function $\alpha(\hat{x};H)$, demonstrating that the approximation captures the dominant trend in the results.

B. Reflectance group delay

The group (or phase-gradient) delay of the cochlear reflectance is the major determinant of the characteristic frequency spacings of OAE fine structure (Shera and Zweig, 1993a; Zweig and Shera, 1995; Talmadge *et al.*, 1998; Shera, 2003a). We have shown previously that integral (54) for R (with $\alpha = 1$) predicts that the reflectance group delay (defined by $\tau \equiv -\partial_\omega \angle R$) is determined by the phase slope of the integrand evaluated near its magnitude peak (e.g., Zweig and Shera, 1995, Appendix D). In the short-wave regime $\alpha(x)$ modifies both the amplitude and phase of the integrand near the peak (see Fig. 5), and we therefore expect reflectance group delays in the 2-D model to differ somewhat from their 1-D values. However, the close match between the phase curves of Fig. 10 suggests that any differences are small.

Figure 12 quantifies group-delay differences between response-matched 1-D and 2-D models using histograms assembled from simulations employing different random distributions of impedance perturbations. Group delays are shown in a dimensionless form representing the number of periods of delay at the emission frequency, which was varied in a small neighborhood about 3 kHz. As expected, the histograms peak at slightly different values, with $\tau_{1\mathrm{d}} < \tau_{2\mathrm{d}}$. Although the modal values are robust, both histograms have substantial width, indicating considerable variability in the results. This variability is manifest both at nearby frequencies in a single (model) ear and between ears at fixed frequency. Similar broad distributions of reflection-source OAE group delay are found experimentally in both human and animal subjects (e.g., Shera and Guinan, 2003, Figs. 1 and 3; Shera, 2003a; Figs. 3 and 4). According to the model, the variability reflects the underlying irregularity in the mechanical perturbations that give rise to the reverse-traveling wave.

To understand the difference between the modal values of $\tau_{1\mathrm{d}}$ and $\tau_{2\mathrm{d}}$, note that the smooth (nonstochastic) component of the integrand ($\mathcal{I}$) in Eq. (54) for R_{Born} can be written in the form

$$\mathcal{I} \equiv \alpha k^2 W_r^2 \sim \alpha \left(\frac{T}{k}\right)^2, \tag{56}$$

where T is the BM mechanical transfer function ($V_{\mathrm{BM}}/V_{\mathrm{stapes}}$) and we have used Eq. (47) with the identification $\bar{P} \sim W_r$. Computing the group delay at the magnitude peak yields

$$\tau \cong \hat{\tau}_{\mathcal{I}} \equiv -\partial_\omega \angle \mathcal{I}|_{\mathrm{peak}} = 2\hat{\tau}_{\mathrm{BM}} - 2\hat{\tau}_k + \hat{\tau}_\alpha, \tag{57}$$

where $\tau_k \equiv -\partial_\omega k$, and so on. In 1-D models, where the peak region is assumed to be long wave, $\alpha \to 1$ and $\tau_\alpha \to 0$. Thus,

$$\tau_{1\mathrm{d}} \cong 2(\hat{\tau}_{\mathrm{BM}} - \hat{\tau}_k). \tag{58}$$

When the peak region is short wave, however, $\alpha \cong \alpha_{\mathrm{WKBs}} \to kH$ [Eq. (52)], so that

$$\tau_{2\mathrm{d}} \cong 2\hat{\tau}_{\mathrm{BM}} - \hat{\tau}_k. \tag{59}$$

The short-dashed lines in Fig. 12 demonstrate that the modal values of $\tau_{1\mathrm{d}}$ and $\tau_{2\mathrm{d}}$ are well approximated by Eqs. (58) and (59).

To determine the sign of $\hat{\tau}_k$, note that wave numbers obtained via inverse analysis in sensitive preparations (e.g., Zweig, 1991; de Boer, 1995b) indicate that $\mathrm{Re}\{k\} > 0$ and that $\mathrm{Im}\{k\}$ goes through a negative-going zero crossing in the vicinity of the response peak (see footnote 2). Using local scaling symmetry to convert these spatial derivatives at fixed frequency into frequency derivatives at fixed position then yields $\hat{\tau}_k > 0$.[10] Consequently,

$$\tau_{1\mathrm{d}} < \tau_{2\mathrm{d}} < 2\hat{\tau}_{\mathrm{BM}}, \tag{60}$$

consistent with the results shown in Fig. 12. Since $\hat{\tau}_k$ is typically only a fraction of $2\hat{\tau}_{\mathrm{BM}}$, the approximation $\tau \cong 2\hat{\tau}_{\mathrm{BM}}$ appears good to within 10%–20%. Inequalities (60) imply that the approximation is improved by short-wave effects within the scattering region. These results are quantitatively consistent with direct and indirect comparisons of SFOAE and BM group delays performed in the basal half of the cochlea (Cooper and Shera, 2004; Shera and Guinan,

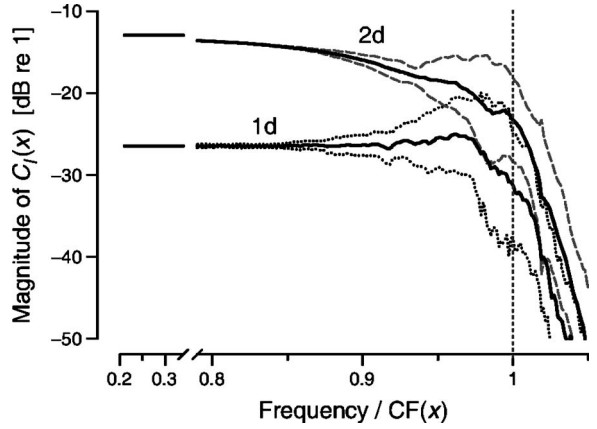

FIG. 13. Wave coefficients $C_l(x)$ in 1-D and 2-D models. Solid lines show the mean magnitudes of 20 numerical computations of $C_l(x)$ computed in response-matched 1-D and 2-D models at fixed frequency. The spatial coordinate x varies along the abscissa; for reference, the peak of the corresponding BM velocity response is marked by the vertical dotted line. In order to emphasize detail in the peak region, the interval (0.34,0.79), over which the functions $C_l(x)$ are almost constant, has been excised from the abscissa. Each of the 20 pairs of 1-D and 2-D simulations employed a different random realization of the impedance perturbations, $\epsilon(x)$. To factor out differences in overall reflectance magnitude due to variations in $\epsilon(x)$, we normalized the functions $C_l(x)$ in each model type to a common value at $x=0$ before computing the mean. Standard deviations about the mean are shown using thinner dashed and dotted lines. Coefficient functions $C_l(x)$ were computed from $\bar{P}(x)$ using the projection operator $\hat{P}_l(x)$ [Eqs. (24) and (25)]. Means and standard deviations were computed after log-transforming the data.

2003). For example, Cooper and Shera (2004) report the relation $\tau_{\mathrm{SFOAE}}=(1.86\pm0.22\,\mathrm{s.d.})\,\hat{\tau}_{\mathrm{BM}}$ based on a comparison of otoacoustic and near-CF mechanical group delays measured in the same ears (ten guinea pigs, one chinchilla).

C. Location of the scattering region

The cochlear reflectance quantifies wave reflection as viewed from just inside the oval window, the intracochlear location where OAEs couple to the middle ear. The projection operators $\hat{P}_{\{r,l\}}(x)$ can, however, be applied at locations throughout the cochlea, not just at $x=0$. In particular, they enable us to locate the region of dominant scattering, even allowing us to look inside the scattering region to determine how the wave amplitudes vary with position.

Figure 13 shows the magnitude of the wave coefficient $C_l(x)$. $C_l(x)$ is defined so that $\bar{P}_l(x)=C_l(x)W_l(x)$, and its value can found from the solution $\bar{P}(x)$ using the equation (see footnote 4)

$$C_l(x)\equiv\frac{\hat{P}_l(x)\{\bar{P}(x)\}}{W_l(x)}, \tag{61}$$

where the projection operator is defined by Eq. (25). The coefficient $C_l(x)$ indicates how the amplitude of the reverse-traveling wave varies with position, and its detailed form depends on the particular distribution of perturbations employed. Here, we highlight general trends by averaging over multiple random realizations of the function $\epsilon(x)$; the irregularity characteristic of individual curves is therefore smoothed out in the mean. In both 1-D and 2-D models, the coefficient $C_l(x)$ rises rapidly from zero over a relatively short interval close to the characteristic place and quickly approaches an almost constant value at locations closer to the stapes. [The corresponding coefficient, $C_r(x)$, for the forward-traveling wave is essentially constant on the scale of the figure.] Since changes in $C_l(x)$ arise via scattering of the forward-traveling wave, the region of dominant scattering occurs where $C_l(x)$ changes rapidly. Scattering in both long- and short-wave models thus occurs principally near the peak of the traveling wave.

Spatial fluctuations in the amplitude of the net reverse-traveling wave due to the random distribution of perturbations produce the large variance in the magnitude of $C_l(x)$ seen within the scattering region. Note, however, that in the 2-D model $C_l(x)$ approaches its final, asymptotic value somewhat more slowly (and smoothly) than it does in the 1-D model. Measured in this way (i.e., in the scalae-averaged pressure), the effective scattering region thus extends somewhat more basally in the 2-D model than it does in 1-D. Because of the breakdown in approximation (41) for $\bar{G}_0(x|x')$ this "near-field" effect is not captured by Eq. (44) for $\bar{P}(x)$.

VII. DISCUSSION

The theory of coherent reflection filtering explains the empirical form for the cochlear reflectance by showing how it emerges from the coherent "backscattering" of forward-traveling waves by random impedance perturbations in the mechanics of the cochlear partition (Shera and Zweig, 1993b; Zweig and Shera, 1995; Talmadge *et al.*, 1998). The theory follows from the analysis of wave scattering in the one-dimensional cochlear model and indicates that at low stimulus intensities the creation of realistic reflection-source OAEs involves three basic principles: First, *the peak of the traveling wave is tall*. As a result, wavelets reflected near the peak have larger amplitudes than those reflected elsewhere, effectively localizing the reflection to the region about the peak. Second, the *peak of the traveling wave is broad relative to the distance between perturbations* (e.g., the width of a hair cell). Consequently, the peak region contains many scattering centers, whose irregular distribution comprises many different spatial frequencies. The many perturbations produce many scattered wavelets, each originating from a different location within the peak, and these wavelets combine and interfere with one another both constructively and destructively. Finally, *the wavelength of the traveling wave is approximately constant over the peak region*. Consequently, wavelets reflected by perturbations arrayed at a particular spatial period undergo a phase change due to scattering that precisely compensates for the phase change due to wave propagation forth and back to the point of reflection (an analog of Bragg's law). Such wavelets therefore combine constructively with one another, and their sum dominates the net reflected wave. The particular spatial period that produces maximal reflection is determined dynamically by the traveling wave. More precisely, coherent backscattering occurs from perturbations arrayed at a spatial period matching half the wavelength of the traveling wave at its peak ($\hat{\lambda}$). Wavelets scattered by spatial-frequency components whose peri-

ods are either considerably larger or smaller than $1/2\hat{\lambda}$ combine incoherently and largely cancel one another out.

Although it successfully accounts for a wide variety of otoacoustic phenomena, the theory of coherent reflection was derived using an assumption about cochlear hydrodynamics (the long-wave assumption) that breaks down near the region of maximal scattering (see Fig. 1). Therefore, to understand how short-wave behavior near the peak of the traveling wave affects the properties of reflection-source OAEs, we have solved the problem of wave scattering by distributed mechanical perturbations in a two-dimensional cochlear model that supports both long and short waves and the transition between the two. Just as in the 1-D theory, we find that the cochlear reflectance can be expressed as an integral representing the summation of wavelets scattered by perturbations located throughout the cochlea. In response-matched models the integrand is identical to the 1-D case, with the exception of an additional factor of $\alpha(x)$ that encapsulates the 2-D hydrodynamics. The function $\alpha(x)$ is defined as the ratio of the difference pressure driving the cochlear partition to the pressure averaged over the scalae cross section [Eq. (18)]. Because $\alpha(x)$ peaks near the characteristic place but has a relatively slowly varying phase (see Fig. 5), it has quantitative but no significant qualitative effects on the analytic structure of the scattering integral. As a result, the physical mechanism of coherent reflection operates essentially unchanged.

Although both Zwislocki's proof and naive application of Siebert's uncoupled equations suggest that wave reflection does not occur in the short-wave regime, our results establish that reflection from the peak region is actually significantly enhanced ($|\alpha| \gg 1$) relative to the long-wave case (Figs. 10 and 11). In effect, the short-wave hydrodynamics act to magnify the apparent size of the perturbations located near the peak of the traveling wave, thereby increasing the amount of scattering. In addition to boosting emission amplitude, short-wave effects also modify the emission group delay (Fig. 12). The group delay sets the rate at which emission phase varies with frequency and is the major determinant of OAE fine-structure spacings (e.g., Talmadge *et al.*, 1998; Shera, 2003a). The short-wave analysis yields slightly longer group delays (τ) and improves the accuracy of the first-order approximation $\tau \cong 2\hat{\tau}_{\mathrm{BM}}$ used to estimate BM group delays from OAE measurements (e.g., Shera and Guinan, 2003; Shera *et al.*, 2002). To second order the analysis predicts $\tau \cong 2\hat{\tau}_{\mathrm{BM}} - \hat{\tau}_k < 2\hat{\tau}_{\mathrm{BM}}$, consistent with direct comparisons of otoacoustic and BM group delays in the basal turns of the cochlea (Cooper and Shera, 2004).

Despite these quantitative differences, the principal qualitative conclusions of the long-wave theory, including its explication of the mechanism of coherent reflection responsible for emission generation, survive intact. The fundamental reason for this is simple: The theory indicates that although the mechanisms of coherent scattering depend strongly on functional characteristics of the traveling-wave peak such as its height, width, and wavelength, they remain relatively insensitive to details of the biophysical processes that determine how that peak originates.

As a corollary, we note that although we have illustrated our findings and procedures with numerical simulations performed using a variant of the model obtained by solving the inverse problem in squirrel monkey (Zweig, 1991), our arguments and conclusions are considerably more general. Indeed, none of them depends on any particular biophysical detail of the model employed. Other models that produce realistic cochlear traveling waves—whether those models be largely phenomenological in character or deduced from first principles involving strings and branes—would serve just as well. As our analytic results make clear, the qualitative form of R depends primarily on the form of the BM velocity response [which determines the wave number, $k(x)$, via Eq. (50)] and not on unknown, model-dependent, or currently controversial micromechanical details concerning the biophysics of force generation within the organ of Corti.

A. The dimensional reduction

The arguments needed to justify the results summarized above require surmounting (or at least circumventing) a number of technical obstacles of interest in their own right. The foundation of the analysis is the observation that OAEs couple to the middle ear via pressures in the long-wave regime averaged across the surface of the stapes. This observation buttressed our early intuition (i.e., hope) that the potentially complicated details of the pressure distribution $P(x,y)$ within the scattering region would ultimately prove unimportant for predicting the value of the reflectance at the stapes. Duifhuis' (1988) averaging procedure then allowed us to reduce the general 2-D problem to an effective 1-D wave equation for the scalae-averaged pressure, $\bar{P}(x)$. This strategy of focusing on a useful level of detail proved successful, since we were then able to find a simple, approximate expression for the reduced traveling-wave Green's function that gives the far-field response to great precision.

The reduced traveling-wave Green's function is derived from a complex-valued (or frequency-domain) Green's function $G(x,y|x',y')$ that differs from the conventional real-valued Green's function often used to describe fluid coupling in the cochlea (e.g., Allen, 1977; Mammano and Nobili, 1993; Parthasarathi *et al.*, 2000; Shera *et al.*, 2004).[11] Although both Green's functions satisfy the equivalent of Eq. (26) and have vanishing normal derivatives at the walls, they differ in the boundary conditions satisfied at the BM. Whereas the conventional Green's function treats the BM as another hard wall (the BM dynamics enter at a later stage), the Green's function introduced here has a normal derivative determined by the smooth component of the BM impedance [see discussion after Eq. (26)]. Thus, unlike the conventional Green's function, our $G(x,y|x',y')$ builds in the collective, wavelike phenomena that emerge from interactions between the cochlear partition and the surrounding fluids. It is therefore well suited for solving linear (or quasilinear) perturbative problems, such as those involving the production of OAEs [for further discussion, see Shera *et al.* (2004)].

As a cautionary note, we point out that an integral equation with the same form as Eq. (29) can be derived by rewriting wave equation (19) for the scalae-averaged pressure in the equivalent inhomogeneous form

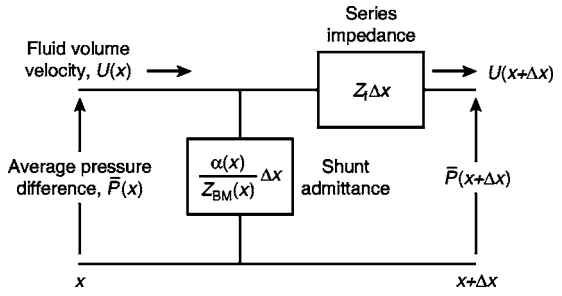

FIG. 14. Equivalent transmission-line analog for a section of the 2-D model of the cochlea of length Δx. The series impedance $Z_f\Delta x$ includes the inertia of the cochlear fluids oscillating in the longitudinal direction. The effective shunt admittance $Y(x)\Delta x$, where $Y(x)=\alpha(x)/Z_{BM}(x)$, characterizes the transverse response of the cochlear partition to the average pressure difference $\bar{P}(x)$. The "current" flowing in the transmission line is the longitudinal component of the fluid volume velocity, $U(x)$.

$$(\partial_x^2+k^2)\bar{P}=-\varrho\bar{P}, \tag{62}$$

so that the mechanical perturbations are isolated on the right-hand side of the equation. If this equation is now naively converted to an integral equation using the one-dimensional, long-wave Green's function $G(x|x')$ [see Eq. (37) and Appendix B], one obtains the (incorrect) relation

$$\bar{P}(x)\overset{\text{☹}}{=}\bar{P}_r(x)+\int_0^\infty G(x|x')\varrho(x')\bar{P}(x')dx', \tag{63}$$

a result identical to Eq. (29) except that the long-wave Green's function, $G(x|x')$, appears in place of the reduced traveling-wave Green's function, $\bar{G}_0(x|x')$. The error in this analysis is that although the pressure $\bar{P}(x)$ satisfies a one-dimensional wave equation, the "sources" $\varrho\bar{P}$ remain inherently two-dimensional—they are located at points *on* the BM rather than being distributed uniformly over y. As outlined in Sec. IV B, the correct procedure for deriving the integral representation for $\bar{P}(x)$ is to derive the integral representation for $P(x,y)$ *before* averaging over y.

B. The equivalent transmission line

The existence of a wave equation for $\bar{P}(x)$ means that the equivalent 1-D system can be represented as a transmission line, a section of which is illustrated in Fig. 14. The dynamical variables are the average pressure difference, $\bar{P}(x)$, and the longitudinal component of the volume velocity, $U(x)$. To find the series impedance and shunt admittance that characterize the line, we begin with Eq. (6),

$$\partial_x\bar{P}=-Z_fU, \tag{64}$$

an equation obtained by averaging the linearized Euler equation over the scalae. Differentiating this equation with respect to x and rewriting the result using Eqs. (19) and (20) yields the equation

$$\partial_xU=-Y\bar{P}, \tag{65}$$

where $Y(x)\equiv\alpha(x)/Z_{BM}(x)$. Equations (64) and (65) represent the pair of coupled first-order equations defining a one-dimensional transmission line with series impedance Z_f and shunt admittance Y, both per unit length (e.g., Slater, 1942). In the long-wave limit $\alpha\to1$ and $Y\to1/Z_{BM}$, so that the system shown in Fig. 14 reduces to the standard equations describing the one-dimensional transmission-line model (e.g., Wegel and Lane, 1924; Zwislocki-Mościcki, 1948; Peterson and Bogert, 1950; Zweig *et al.*, 1976).

Do short-wave effects modify the effective scalae area?

The equivalent transmission line illustrated in Fig. 14 associates the factor α with the BM impedance, using it to define an effective admittance, $Y\leftarrow\alpha/Z_{BM}$. But from the perspective of the definition $k^2=-\alpha Z_f/Z_{BM}$ [Eq. (20)] and the derivation preceding it, the factor α might just as well have been associated with the impedance Z_f and used to define an effective fluid impedance $Z_{eff}\leftarrow\alpha Z_f$. In this latter case, the factor α would act to modify the effective scalae area and hence the acoustic mass (mass density per cross-sectional area) associated with fluid movement in the duct. In this view, Eq. (8) for Z_f would naturally be rewritten to read

$$Z_{eff}(x)\equiv2i\omega\rho_0/S_{eff}(x), \tag{66}$$

where $S_{eff}(x)=bH_{eff}(x)$, with $H_{eff}(x)\equiv H/\alpha(x)$. Since $\alpha(x)$ is essentially real basal to $\hat{x}$ and increases with distance from the stapes, the effective height $H_{eff}(x)$ tapers down toward the characteristic place;[12] the effective acoustic mass $\rho_0/S_{eff}(x)$ therefore increases correspondingly. Although this formulation has considerable intuitive appeal, the notion that short-wave effects can be regarded as reducing the effective height or cross-sectional area of the scalae (e.g., Zwislocki, 1983, 2002; Hubbard and Mountain, 1996) cannot be used to find the equivalent one-dimensional wave equation. The derivation outlined above implies that Fig. 14, in which α modifies Z_{BM} rather than Z_f, uniquely specifies the equivalent transmission line.

Although mistakenly associating the factor α with the impedance of the fluid rather than with the impedance of the BM has no effect on the wave number, it does modify the apparent characteristic impedance of the system.[13] In particular, the characteristic impedance becomes $Z_0=\sqrt{\alpha}Z_0^{lw}$ (where $Z_0^{lw}=\sqrt{Z_fZ_{BM}}$), which differs by a factor of $\alpha(x)$ from its actual value, $Z_0^{lw}/\sqrt{\alpha}$. Since $\alpha\cong\alpha_{WKBs}\to-H^2Z_f/Z_{BM}$ in the short-wave limit [see Eqs. (51) and (52)], the (incorrect) characteristic impedance approaches $Z_0\to-iHZ_f=2\omega\rho/b$, a value independent of Z_{BM}.[14]

Recall from the Introduction that Zwislocki (1983, 2002) applied this counter-intuitive and evidently erroneous result—namely, the apparent cancellation of all factors of Z_{BM} in the short-wave formula for Z_0—to deduce that wave reflection arising from spatial variations in the BM impedance cannot occur in the short-wave regime. The error in Zwislocki's argument is that no such cancellation occurs when the series impedance and shunt admittance of the equivalent transmission line are correctly identified.[15]

C. Need for the inverse procedure

Another crucial component of our argument follows from the recognition that meaningful comparisons between models of different heights or dimensionality require control-

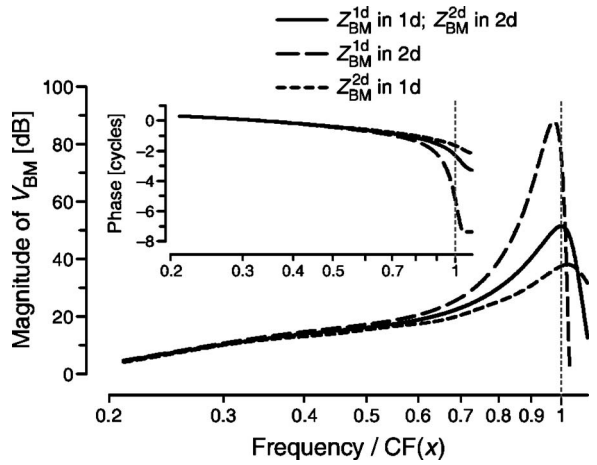

FIG. 15. Results of model cross-breeding. The panels show the BM velocity responses computed by crossing 1-D and 2-D models and their respective impedances, $Z_{BM}^{1d}(x)$ and $Z_{BM}^{2d}(x)$, taken from Fig. 9. All four possible combinations of model/impedance are shown. The solid lines show the normal, ''homozygous'' cases (i.e., 1-D/1-D and 2-D/2-D), reproduced from the top panel of Fig. 9. The two homozygous cases are indistinguishable on the scale of the graph. The long dashed lines show the heterozygous case 1-D/2-D, and the short dashed lines show the case 2-D/1-D. BM velocity magnitudes are shown in the main panel, phases in the inset. For reference, vertical dotted lines locate the peak of the target (i.e., homozygous) BM velocity response along the abscissae.

ling for variations in mechanical tuning that occur when the geometry of the model is varied with $Z_{BM}(x)$ held fixed. Although differences between $Z_{BM}^{1d}(x)$ and $Z_{BM}^{2d}(x)$ appear relatively minor in the context of Fig. 9, they nonetheless have striking functional consequences, as demonstrated in Fig. 15, which plots the ''mutant'' responses that result from model ''cross-breeding'' (e.g., computing V_{BM} in a 2-D model using the 1-D impedance and vice versa).[16] Corresponding to the sizable amplitude differences illustrated in the main panel are large differences in response phase (inset) that greatly affect the reflectance group delay. Unless controlled for using an inverse procedure such as that outlined here, these fundamental differences in the basic response properties of the model would hopelessly swamp the relatively small differences in OAE characteristics actually attributable to short- versus long-wave scattering.

In the one-dimensional model, Eq. (50)—or Zweig's (1991) WKB-based method for finding the wave number—provides a complete solution to the inverse problem because the BM impedance can be found from $k^2(x)$ using the equation $Z_{BM}^{1d}(x) = -Z_f/k^2(x)$, obtained from Eq. (51) with $\alpha = 1$. (The fluid impedance Z_f is set by the model geometry and is assumed known.) But the solution remains incomplete in 2-D because $\alpha(x)$, and the information it encodes about hydrodynamic contributions to the response, remains undetermined. For this reason, we need to supplement the wave number inversion with a procedure to determine $\alpha(x)$; the iterative method illustrated in Fig. 8 solves this problem.

Although applied here within the specific context of the 2-D scattering problem, the inversion procedure developed in Sec. V provides an alternative to existing inverse methods in the literature. The BM velocity response $V_{BM}(x)$ that serves as input to the procedure can be obtained experimentally either by direct spatial measurement (e.g., Ren, 2002) or by transforming frequency-domain measurements to the place domain with the aid of approximate symmetries such as scaling (e.g., Zweig, 1976). Although a number of technical issues complicate the inversion procedure when applied to experimental data sets (cf. Zweig, 1991; de Boer, 1995a,b; de Boer and Nuttall, 1999),[17] none of them compromises the conclusions of this paper.

D. Review of the assumptions

To derive the results reported here we employed a number of simplifying assumptions. For example, rather than labor under the added complexity of the full three-dimensional, coiled, asymmetric, tapered geometry of the actual cochlea, we deliberately adopted the simplest geometry that manifests both short- and long-wave behavior (i.e., the symmetric 2-D box model). Although these geometric restrictions can be relaxed [e.g., Duifhuis' (1988) dimensional reduction procedure was originally applied to a 3-D model; see also Talmadge *et al.* (2001)], we see no reason to expect that the effort will produce anything but minor quantitative changes to the results. We have shown elsewhere that the long-range (far-field) hydrodynamics of an uncoiled but otherwise realistic 3-D model (Mammano and Nobili, 1993) are captured by a simple, one-dimensional transmission line (Shera *et al.*, 2004, Appendix A). And in the short-wave regime near the peak of the traveling wave the pressure field decreases rapidly with distance from the cochlear partition (e.g., Olson, 2001), so that the precise geometry of the scalae walls becomes unimportant. These hand-waving physical arguments are corroborated by computations showing that mechanical perturbations introduced into a 3-D model for the purposes of simulating SOAEs produce results in accord with the theory of coherent reflection (de Boer *et al.*, 2004).

Since our goal has been to understand short- versus long-wave effects on the cochlear reflectance R, rather than provide a description of reflection-source OAEs as measured in the ear canal, we assumed for simplicity [e.g., in obtaining Eq. (44) from Eq. (43)] that the stapes presents a perfectly reflectionless boundary to reverse-traveling waves ($R_{stapes} = 0$). Since reflection from the stapes occurs in the long-wave regime, the effects of multiple internal reflection (e.g., the production of intracochlear standing waves, small systematic shifts in fine-structure spacings, etc.) carry over from previous analyses (e.g., Talmadge *et al.*, 1998; Dhar *et al.*, 2002; Shera, 2003a).

The model assumes that the mechanical properties of the cochlear partition vary irregularly (i.e., nonsmoothly) with position. This assumption is consistent with general arguments that locate the origin of reflection-source OAEs in preexisting (place-fixed) mechanical perturbations in the organ of Corti (Kemp and Brown, 1983; Shera and Guinan, 1999). In the ear, the precise nature of these perturbations remains unknown, although spatial variations in hair-cell number and geometry (Engström *et al.*, 1966; Bredberg, 1968; Wright, 1984; Lonsbury-Martin *et al.*, 1988)—and perturbations not so visible in the anatomy, such as variations in OHC forces due to random, cell-to-cell variations in the number of OHC motor proteins—all presumably contribute.

The perturbations used here were introduced by "jiggling" the poles of the BM admittance randomly with position (see Appendix D). However, none of our conclusions depend on the precise form of the perturbations; other schemes (such as jiggling the real or imaginary parts of the BM impedance, jiggling the "active" part of the impedance, jiggling particular model parameters, etc.) give similar results. Although the model assumes for simplicity that the BM impedance changes discontinuously (e.g., from hair cell to hair cell), equivalent results are obtained with much smoother patterns so long as the "roughness" contains spatial frequencies within the passband of the "spatial-frequency filter" that arises through the dynamical action of the traveling wave (see Zweig and Shera, 1995, Figs. 6 and 10).

Considerable evidence indicates that the production of low-level evoked and spontaneous OAEs involves the biophysical and hydromechanical mechanisms that serve to amplify the motion of the basilar membrane. We have therefore assumed that active forces exerted within the cochlear partition couple primarily into the transverse motion of the partition, and thereby into the classical traveling pressure wave that drives it. As a result, we have neglected the possibility that the accelerations of structures within the organ of Corti (e.g., the outer hair cells) also produce significant acoustic compressional waves that propagate through the cochlear fluids at the speed of sound uninfluenced by the basilar membrane (or other tuned mechanical structures, in the case of nonmammalian tetrapods such as frogs and lizards). In principle, back propagation via compressional waves provides an additional mechanism for energy to escape from the inner ear, and mounting albeit not unequivocal evidence suggests that the mechanism operates in the mammalian ear (e.g., Wilson, 1980; Ren, 2004; Ruggero, 2004). Emissions due to compressional waves presumably mix and interfere with those propagated via the transverse pressure difference wave, and their relative amplitudes must depend on factors not currently known with any certainty (e.g., the magnitude of the mechanical perturbations and the strength of any compressional sources). Despite differences in the mechanisms of back propagation, we nevertheless find that the principal physical mechanisms operating in the coherent reflection model (e.g., mechanical irregularity, phase-coherent summation, and dynamical spatial-frequency filtering) also play an important role in shaping the characteristics of any "compressional-wave" OAEs (Shera *et al.*, 2005).

Finally, since the model underlying our analysis is linear, its region of validity is strictly limited to the low-level linear regime near the threshold of hearing. Nevertheless, just as with the 1-D analysis, we expect that many of the more qualitative concepts of the theory will continue to apply, mutatis mutandis, at higher intensities. Furthermore, the 2-D scattering formalism developed here can easily be generalized—just as it was in 1-D (e.g., Talmadge *et al.*, 2000; Shera, 2003b)—to provide a framework for investigating perturbative nonlinear effects, such as "nonlinear roughness" and the generation of distortion products.

E. Effects of scalae height revisited

Our finding that short-wave hydrodynamics enhance the reflection of traveling waves subverts the introductory speculation that the scalae evolved their curiously large size in order to suppress unwanted reflections. If we assume that oversized scalae are conserved not as developmental spandrels (Gould and Lewontin, 1979) but via selective pressure from some direct adaptive advantage, then whatever detriments to cochlear signal processing follow from the increased reflection must be offset by other benefits that accrue to the organism. One obvious possibility is that large scalae confer homeostatic and protective benefits as buffers that help to dampen fluctuations in ionic concentrations.

But another possibility suggested by our analysis is that scalae size plays an important role in shaping the characteristics of cochlear tuning. The mutant BM velocity responses shown in Fig. 15 demonstrate that large changes in mechanical tuning can be produced even when the "active elements" in cochlear mechanics (the BM impedance functions) are held invariant. For example, when the impedance $Z_{\mathrm{BM}}^{1\mathrm{d}}(x)$ is used in the 2-D model the gain of the BM velocity response increases substantially. And vice versa—when $Z_{\mathrm{BM}}^{2\mathrm{d}}(x)$ is employed in a context where the hydrodynamics are effectively one-dimensional the BM velocity response decreases. The dimensions of the scalae in which the organ of Corti finds itself embedded therefore directly affect the sensitivity and bandwidth of mechanical tuning. These results illustrate the power of global hydrodynamic effects in cochlear mechanics. Since scalae sizes vary considerably across species (e.g., Thorne *et al.*, 1999), purely geometric and hydromechanical factors unrelated to active processes or micromechanics within the organ of Corti may make significant contributions to observed species differences in OAE amplitudes and cochlear tuning (e.g., Zurek, 1985; Probst *et al.*, 1991; Shera *et al.*, 2002; Oxenham and Shera, 2003).

ACKNOWLEDGMENTS

We thank Stephen Neely for generously sharing his finite-difference algorithms and thereby providing an independent check on our numerical solutions. We also thank Egbert de Boer, Paul Fahey, John Guinan, Robert Withnell, and the two anonymous reviewers for their helpful comments on the manuscript. This work was supported by Grant Nos. R01 DC003687 (CAS) and R01 DC003094 (CLT) from the NIDCD, National Institutes of Health.

APPENDIX A: FINDING THE BASIS WAVES

The basis waves $W_{\{r,l\}}(x)$ are defined as solutions to Eq. (23) and represent the two independent traveling-wave solutions in the smooth cochlea (Shera and Zweig, 1991; Talmadge *et al.*, 1998). Knowledge of the basis waves is necessary for finding the projection operators $\hat{P}_{\{r,l\}}$ [Eq. (25)], for determining R_{stapes} from a given load impedance at the oval and round windows, and for computing the traveling wave Green's function [Eq. (41) and Appendix B]. Determining the form of the basis waves is therefore central to any discussion of bi-directional wave propagation in the cochlea.

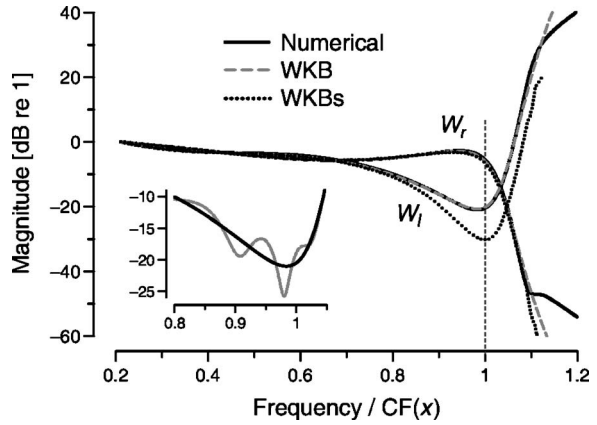

FIG. 16. The basis waves $W_{\{r,l\}}(x)$, numerically and approximately computed. The main panel shows the magnitudes $|W_{\{r,l\}}(x)|$ computed numerically (solid lines) using the procedures outlined in the text. The panel also shows two alternative forms of the WKB basis waves. The dashed gray line shows the functions $W^{\mathrm{WKB}}_{\{r,l\}}(x)$ derived here [Eq. (A3)]; the dotted line shows the functions $W^{\mathrm{WKBs}}_{\{r,l\}}(x)$ [Eq. (A4)] derived by integrating the "standard" WKB approximation for the 2-D model over the scalae height. For reference, a vertical dotted line locates the peak of the corresponding BM velocity response along the abscissa. Inset: The inset shows the numerical solution for $W_l(x)$ (gray line) obtained using the initial estimate for Δ [namely, $-2i\ \mathrm{Im}\{W_r'(0)\}\cong 0.843i\ \mathrm{mm}^{-1}$]. The numerical solution from the main panel, reproduced for comparison (black line), was obtained by varying Δ to minimize the integrated curvature of the solution [Eq. (A2)]. The minimum curvature occurs at $\Delta\cong -0.048+0.85i\ \mathrm{mm}^{-1}$; for comparison, $\Delta(W_r^{\mathrm{WKB}}, W_l^{\mathrm{WKB}})=2ik_0\cong -0.04+0.84i\ \mathrm{mm}^{-1}$.

1. Numerical computation of the basis waves

In a smooth cochlea, forward-traveling waves normally undergo negligible internal reflection (e.g., Shera and Zweig, 1991), so that the basis wave $W_r(x)$ can readily be obtained by solving the model equations with a stimulus applied at the stapes (see Fig. 16). Numerical computation of the reverse-traveling basis wave $W_l(x)$ can be substantially more difficult, however, because wave reflection at the stapes complicates the computation of a pure reverse-traveling solution (Shera and Zweig, 1991).

Perhaps the most straightforward approach to computing $W_l(x)$ numerically is to apply d'Alembert's reduction of order method (e.g., Ince, 1956), which allows a second independent solution to be determined if the first is known. When applied to the wave equation (23) the method yields the explicit formula

$$W_l(x;\Delta)=W_r(x)\left[1+\Delta\int_0^x\frac{dx'}{W_r^2(x')}\right], \tag{A1}$$

where the adjustable complex constant Δ sets the Wronskian determinant $\Delta(W_r,W_l)$ and the constant of integration has been chosen so that $W_l(0)=1$. Although the solution $W_l(x;\Delta)$ given by Eq. (A1) is linearly independent of $W_r(x)$, it does not necessarily represent a *pure* reverse-traveling wave. Unless Δ is chosen so that $W_l(x;\Delta)$ satisfies no-reflection boundary conditions at the stapes, the solution will be a mixture of forward- and reverse-traveling waves.[18]

To obtain a pure reverse-traveling wave we need to minimize boundary reflection by adjusting Δ so that $W_l(0)/W_l'(0)$ is proportional to the "wave impedance" of a reverse-traveling wave at the stapes (Shera and Zweig, 1991; Viergever and de Boer, 1987).[19] A reasonable first approximation is to set $W_l'(0)$ equal to the complex conjugate of $W_r'(0)$, yielding the estimate $\Delta\cong[W_r'(0)]^*-W_r'(0)=-2i\,\mathrm{Im}\{W_r'(0)\}$. The amplitude of any residual forward-traveling component can often be significantly reduced by varying the value of Δ in a neighborhood about this initial estimate. Note, for example, that contamination of the resulting solution for $W_l(x)$ by a reflected forward-traveling wave component produces standing-wave-like oscillations in the magnitude and phase of $W_l(x)$ (see Fig. 16, inset). Since any standing-wave component increases the total curvature of the solution, adjusting Δ to minimize the value of

$$\kappa^2(\Delta)\equiv\int|\partial_x^2[W_lW_r]|^2\,dx, \tag{A2}$$

where κ^2 measures the integrated squared curvature, often works well in practice (Fig. 16, inset). Note that before computing the second derivative we multiply W_l by W_r in order to maximize the standing-wave contribution to κ^2 by dividing out as much of the secular curvature in W_l as possible. Our choice of divisor is based on the expectation that to zeroth order $W_l\sim 1/W_r$. Alternatively, one could estimate $W_l(x)$ using the WKB approximation (see below) and then minimize the total curvature of the ratio W_l/W_l^{WKB}.

Figure 16 shows the basis waves $W_{\{r,l\}}(x)$ computed using the numerical procedures outlined above (solid lines). The amplitude notch/plateau visible in the cutoff region apical to the characteristic place betrays the influence of non-propagating modes in the pressure (e.g., de Boer and Viergever, 1982; Watts, 2000). The inset illustrates the substantial reduction in standing-wave amplitude [i.e., unwanted mixing of forward- and reverse-traveling waves in the solution $W_l(x)$] that can be achieved by minimizing the integrated curvature, $\kappa^2(\Delta)$.

2. Approximate WKB basis waves

Applying the first-order WKB approximation (e.g., Bender and Orszag, 1978; Fröman and Fröman, 1965) to Eq. (23) yields the basis waves

$$W^{\mathrm{WKB}}_{\{r,l\}}(x)=\sqrt{\frac{k_0}{k(x)}}\exp\left(\mp i\int_0^x k(x')dx'\right), \tag{A3}$$

where $k_0\equiv k(0)$. Note that these basis waves differ from those obtained by averaging the "standard" WKB expression for $P(x,y)$ (e.g., Steele and Taber, 1979; Viergever, 1980) over the duct cross-section, which yields

$$W^{\mathrm{WKBs}}_{\{r,l\}}(x)=\frac{A[k_{\mathrm{eik}}(x)H]}{A[k_{\mathrm{eik}}(0)H]}\exp\left(\mp i\int_0^x k_{\mathrm{eik}}(x')dx'\right), \tag{A4}$$

where the amplitude prefactor A has the form

$$A(\eta)\equiv\frac{\sinh(\eta)}{\eta\sqrt{2\eta+\sinh(2\eta)}}. \tag{A5}$$

Note that the wave numbers $k(x)$ and $k_{\mathrm{eik}}(x)$ appearing in Eqs. (A3) and (A4) are not identical. Whereas the wave number $k(x)$ is given by Eq. (20) with $\epsilon=0$, the wave num-

ber $k_{\mathrm{eik}}(x)$ is defined as the principal solution to the complex dispersion relation

$$k_{\mathrm{eik}}H\tanh(k_{\mathrm{eik}}H)=(k_{\mathrm{lw}}H)^2=-H^2Z_{\mathrm{f}}/Z_{\mathrm{BM}}. \tag{A6}$$

Sometimes referred to as the "eikonal equation," dispersion relation (A6) is equivalent to Eq. (20) evaluated under the additional assumption that $\alpha(x)=\alpha_{\mathrm{WKBs}}(x)$ [i.e., that approximation (52) is exact]. Although the transcendental equation has infinitely many solutions (due to the periodicity of the hyperbolic tangent along the imaginary axis), the principal solution is that which satisfies $k_{\mathrm{eik}}(x)\rightarrow k_{\mathrm{lw}}(x)$ in the basal, long-wave region of the cochlear response. Other solutions can become important in the cutoff-region apical to the traveling-wave peak (e.g., de Boer and Viergever, 1982; Watts, 2000). Using Eq. (20) to express $k_{\mathrm{lw}}(x)$ in terms of $k(x)$ shows that the two wave numbers are related via the equation

$$k_{\mathrm{eik}}H\tanh(k_{\mathrm{eik}}H)=(kH)^2/\alpha. \tag{A7}$$

Since $\alpha_{\mathrm{WKBs}}(x)$ is only approximately equal to $\alpha(x)$, the wave number $k_{\mathrm{eik}}(x)$ is only approximately equal to the wave number $k(x)$.

Figure 16 compares $W^{\mathrm{WKB}}_{\{r,l\}}(x)$ and $W^{\mathrm{WKBs}}_{\{r,l\}}(x)$ to the basis waves computed numerically. As illustrated in the figure, the WKB solutions $W^{\mathrm{WKB}}_{\{r,l\}}(x)$ provide excellent analytic approximations to both the forward- and reverse-traveling basis waves. The standard approximations $W^{\mathrm{WKBs}}_{\{r,l\}}(x)$, however, are less uniformly successful. Although $W^{\mathrm{WKBs}}_{r}(x)$ hugs the forward-traveling basis wave quite closely, the corresponding approximation for the reverse-traveling wave, $W^{\mathrm{WKBs}}_{l}(x)$, deviates from the numerical result quite significantly near the characteristic place.

The amplitude prefactor $A(k_{\mathrm{eik}}H)$ that multiplies the complex exponential in Eq. (A4) is most readily derived using energy-flow arguments (e.g., de Boer and Viergever, 1984; Watts, 1992). Since the derivation assumes an approximate form of the wave number [namely, $k_{\mathrm{eik}}(x)$], the functional form of the prefactor must necessarily be distorted to compensate for this approximation if the overall solution is to remain consistent with energy conservation. The comparison in Fig. 16 indicates that this compensatory distortion works well for forward-traveling waves but fails for waves traveling back toward the stapes. Evidently, the $W^{\mathrm{WKBs}}_{\{r,l\}}(x)$ are not optimal approximate solutions to Eq. (23).

Problems with the standard approximations $W^{\mathrm{WKBs}}_{\{r,l\}}(x)$ might have been anticipated by noting that unlike the waves $W^{\mathrm{WKB}}_{\{r,l\}}(x)$, the functions $W^{\mathrm{WKBs}}_{\{r,l\}}(x)$ have a nonconstant Wronskian determinant; thus, according to the Abel identity (e.g., Ince, 1956; Bender and Orszag, 1978), they cannot be exact solutions to *any* Helmholtz equation.

APPENDIX B: THE LONG-WAVE GREEN'S FUNCTION $G(x|x')$

The long-wave Green's function $G(x|x')$ is the symmetric solution to the equation

$$(\partial_x^2+k^2)G=-\delta(x-x'), \tag{B1}$$

subject to the boundary conditions imposed on the waves in the cochlea. To find $G(x|x')$ we note that the point source $\delta(x-x')$ splits the cochlea naturally into two regions: the basal region between the stapes and the source at x', and the apical region between x' and the helicotrema.[20] In each region the general solution consists of a superposition of basis waves $W_{\{r,l\}}(x)$ traveling in opposite directions. The Green's function is therefore given by an expression of the form

$$G(x|x')=\begin{cases} b_rW_r(x)+b_lW_l(x) & \text{for } x<x', \\ a_rW_r(x)+a_lW_l(x) & \text{for } x>x'. \end{cases} \tag{B2}$$

The constants $a_{\{r,l\}}$ and $b_{\{r,l\}}$ (named for "apical" and "basal," respectively) are chosen so that $G(x|x')$ satisfies matching conditions at x' and any boundary conditions at the ends of the cochlea.

To construct the Green's function we begin by rewriting Eq. (B2) in the simplified form

$$G(x|x')\propto\begin{cases} w_b(x) & \text{for } x<x', \\ w_a(x) & \text{for } x>x'. \end{cases} \tag{B3}$$

Here, the function $w_b(x)$ represents a linear combination of basis waves chosen to satisfy the basal boundary condition imposed at the cochlear boundary with the middle ear. For example, if reverse-traveling waves incident on the stapes are reflected with reflection coefficient R_{stapes} (Shera and Zweig, 1991; Talmadge *et al.*, 1998; Puria, 2003; Shera *et al.*, 2004), then $b_r=R_{\mathrm{stapes}}b_l$, so that $w_b(x)$ has the form $b_l[W_l(x)+R_{\mathrm{stapes}}W_r(x)]$. Likewise, the function $w_a(x)$ represents another linear combination chosen to satisfy the apical boundary condition at the helicotrema. The function $G(x|x')$ in Eq. (B3) thus satisfies the appropriate (although as yet unspecified) boundary conditions at both ends of the cochlea.

The matching conditions can be obtained by integrating Eq. (B1) for $G(x|x')$ over an interval containing x' and taking the limit as the interval shrinks to zero; at x' they require that $G(x|x')$ be continuous and that $\partial_xG(x|x')$ have a unit step discontinuity arising from the delta-function source (e.g., Friedman, 1956). After imposing the matching conditions one obtains

$$G(x|x')=w_b(x_<)w_a(x_>)/\Delta(w_a,w_b), \tag{B4}$$

where $x_<(x,x')\equiv\min(x,x')$ and $x_>(x,x')\equiv\max(x,x')$. The function $\Delta(w_a,w_b)$ is the Wronskian determinant of $w_a(x)$ and $w_b(x)$, defined by

$$\Delta(w_a,w_b;x)\equiv w_a(x)w_b'(x)-w_a'(x)w_b(x), \tag{B5}$$

where the primes denote derivatives. Since $w_a(x)$ and $w_b(x)$ are solutions of a 1-D wave equation [Eq. (19)], the Abel identity implies that $\Delta(w_a,w_b;x)$ is independent of x (e.g., Ince, 1956; Bender and Orszag, 1978); the Wronskian can therefore be evaluated at any convenient point.[21]

If the constants a_l and b_r in Eq. (B2) are both zero, the cochlea is effectively infinite in extent (i.e., waves incident upon its boundaries are not reflected). The long-wave Green's function then becomes

$$G_\infty(x|x')=\gamma W_l(x_<)W_r(x_>), \tag{B6}$$

where

$$1/\gamma \equiv \Delta(W_r, W_l). \tag{B7}$$

If reflections occur at the stapes ($b_r = R_{\text{stapes}} b_l$), the Green's function becomes

$$G(x|x') = G_\infty(x|x') + \gamma R_{\text{stapes}} W_r(x) W_r(x'). \tag{B8}$$

APPENDIX C: THE REDUCED GREEN'S FUNCTION $\bar{G}_0(x|x')$

To illustrate and justify the more heuristic discussion in the text we construct an analytic expression for the reduced traveling-wave Green's function $\bar{G}_0(x|x')$ in the simple case where the BM impedance is independent of position. Our construction generalizes to yield an approximate expression valid when the BM impedance varies sufficiently slowly with position.

We first consider the set of functions $Y_n(y)$ defined by

$$(\partial_y^2 - k_n^2) Y_n(y) = 0 \quad (n = 1,2,...) \tag{C1}$$

and subject to the standard boundary conditions at the top and bottom of the scala:

$$\partial_y Y_n|_{y=H} = 0 \tag{C2}$$

and

$$\partial_y \ln Y_n|_{y=0^+} = H Z_f / Z_{\text{BM}}. \tag{C3}$$

The wave numbers k_n are assumed constant (independent of x and y) with $\text{Re}\{k_n\} > 0$. The functions $Y_n(y)$ are given explicitly by

$$Y_n(y) = C_n \cosh[k_n(H-y)], \tag{C4}$$

with

$$k_n H \tanh[k_n H] = -H^2 Z_f / Z_{\text{BM}} \equiv (H k_{\text{lw}})^2. \tag{C5}$$

If the constants C_n are taken to be

$$C_n = [2/(H + \sinh(2k_n H)/2k_n)]^{1/2}, \tag{C6}$$

then

$$\int_0^H Y_n(y) Y_m(y) dy = \delta_{nm}, \tag{C7}$$

where δ_{nm} is the Kronecker delta; the $Y_n(y)$ therefore form a bi-orthogonal set (e.g., Morse and Feshbach, 1953, Part I, pp. 884–886). Passing over some delicate mathematical issues related to establishing the completeness of the $Y_n(y)$ on the interval $(0,H)$ (see, e.g., Dunford and Schwartz, 1971), we assume the closure relation

$$\sum_{n=1}^{\infty} Y_n(y) Y_n(y') = \delta(y - y'). \tag{C8}$$

A particular solution to Laplace's equation is given by

$$P(x,y) = X_n(x) Y_n(y), \tag{C9}$$

where the functions $X_n(x)$ satisfy the wave equation

$$(\partial_x^2 + k_n^2) X_n(x) = 0. \tag{C10}$$

By introducing the right- and left-moving wave solutions $X_{n;\{r,l\}}(x) \equiv e^{\mp i k_n x}$, we can construct a family of one-dimensional Green's functions, $g_n(x|x')$, defined by

$$(\partial_x^2 + k_n^2) g_n(x|x') = -\delta(x - x'), \tag{C11}$$

with $g_n(x|x') = g_n(x'|x)$. We assume no-reflection boundary conditions so that $g_n(x|x')$ takes the form of waves traveling *away* from the source at x': that is, $g_n(x|x') \sim X_{n;r}(x)$ for $x > x'$ and $g_n(x|x') \sim X_{n;l}(x)$ for $x < x'$. Constructing the Green's function using the procedure outlined in Appendix B yields

$$g_n(x|x') = \frac{1}{2ik_n} e^{-ik_n|x-x'|}. \tag{C12}$$

The 2-D hydrodynamic Green's function may now be represented as

$$G(x,y|x',y') = \sum_{n=1}^{\infty} g_n(x|x') q_n(y|y'), \tag{C13}$$

where $q_n(y|y') \equiv Y_n(y) Y_n(y')$. The procedure outlined in the text (Sec. IV B 2) can now be used to construct integral representations of $P(x,y)$ and $\bar{P}(x)$ with the same form as Eqs. (28) and (29). The reduced Green's function is given by Eq. (30); evaluating the integral yields

$$\bar{G}_0(x|x') = -iH \sum_{n=1}^{\infty} C_n^2 \frac{\sinh(2k_n H)}{2k_n H} e^{-ik_n|x-x'|}. \tag{C14}$$

To obtain an approximate expression for $\bar{G}_0(x|x')$ generalizable to the more realistic case of a nonconstant BM impedance we assume that any $n > 1$ modal contributions to $P(x,y)$ are negligible and approximate $G(x,y|x',y')$ using only the $n = 1$ term in Eq. (C13). Substituting into Eq. (30) then yields

$$\bar{G}_0(x|x') \cong g_1(x|x') Y_1(0^+;x') \int_0^H Y_1(y;x) dy, \tag{C15}$$

where we have included x or x' among the list of independent variables for Y_1 as a bookkeeping device. Note that in this approximation $\alpha(x) \cong Y_1(0^+;x)/\bar{Y}_1(;x)$, where $\bar{Y}_1(;x)$ is the scalae-averaged value of $Y_1(y;x)$. Equation (C15) therefore becomes

$$\bar{G}_0(x|x') \cong g_1(x|x') \alpha(x') \bar{Y}_1(;x') H \bar{Y}_1(;x). \tag{C16}$$

We define the scalae-averaged basis waves as

$$W_{\{r,l\}}(x) \equiv X_{1;r,l}(x) \bar{Y}_1(;x)/\bar{Y}_1(;0), \tag{C17}$$

where the factor $\bar{Y}_1(;x)/\bar{Y}_1(;0)$, everywhere equal to 1 when Z_{BM} is constant, is included to guide generalization to the more realistic case. Equation (C16) can then be written

$$\bar{G}_0(x|x') \cong H \bar{Y}_1^2(;0) \alpha(x') G_\infty(x|x'), \tag{C18}$$

where $G_\infty(x|x')$ is given by Eq. (B6) and the corresponding Wronskian determinant has been evaluated at $x = 0$ assuming that the basal region of the cochlea is long-wave. (When Z_{BM} is constant, $k_n H$ is constant throughout the cochlea.) The same assumption implies that $\bar{Y}_1^2(;0) \cong C_1^2 \cong 1/H$. Thus,

$$\bar{G}_0(x|x') \cong \alpha(x') G_\infty(x|x'). \tag{C19}$$

The reduced traveling-wave Green's function thus agrees with the approximation obtained heuristically in Eq. (41).

Although it is not generally possible to derive an analytic representation of the 2-D hydrodynamic Green's function for the case of an x-dependent BM impedance, an approximate representation can be obtained if we assume that $Z_{\mathrm{BM}}(x)$ varies sufficiently slowly with x. In this case, the $Y_n(y)$ defined by Eqs. (C1)–(C3) depend on x as well as y, and are written as $Y_n(y;x)$, where the x is now more than a bookkeeping device. If we then assume a particular solution of Laplace's equation of the form (C9) and neglect the x derivatives of $Y_n(y;x)$, we again obtain Eq. (C10), but now as an approximate relationship. Construction of the approximate Green's functions $G(x,y|x',y')$ and $\bar{G}_0(x|x')$ then proceeds essentially as before. We assume the validity of these generalized constructions in this paper and show that the results derived from them are in impressive agreement with those obtained from direct finite-difference solutions of the 2-D cochlear-model equations (e.g., Figs. 6 and 10).

APPENDIX D: MODELING DETAILS

1. Form and parameters of the wave number

We adopt a variant of the wave number obtained by solving the inverse problem in squirrel monkey (Zweig, 1991). In particular, the model k^2 has the form

$$k^2(x,\omega)=k^2[\beta(x,\omega)]=\frac{(4N/l)^2\beta^2}{1-\beta^2+i\delta\beta+\rho e^{-2\pi i\mu\beta}}. \tag{D1}$$

The scaling variable $\beta(x,\omega)$ is defined by $\beta(x,\omega)\equiv\omega/\omega_{\mathrm{r}}(x)$, where $\omega_{\mathrm{r}}(x)=2\pi f_{\mathrm{r}}(x)$. The frequency $f_{\mathrm{r}}(x)$ is the undamped, *in vacuo* resonant frequency of the partition [i.e., the resonant frequency in the limit when δ and ρ (see below) are both negligible] and is assumed to vary exponentially with position. Thus, $f_{\mathrm{r}}(x)=f_{\mathrm{r}}(0)e^{-x/l}$ with $l\cong 7$ mm, based on estimates of the human cochlear map (Greenwood, 1961, 1990). The dimensionless parameter N represents the approximate number of wavelengths of the traveling wave on the basilar membrane produced by sinusoidal stimulation (Zweig *et al.*, 1976; Zweig, 1991). The dimensionless parameter δ determines the net damping in the model, and the dimensionless parameters ρ and μ characterize, respectively, the strength and the time delay (in periods of the local resonant frequency) of the stabilizing feedback force.

For ease of analysis, the model variant used here has the same functional form as Zweig's original, but differs somewhat in its parameter values. In particular, we use the simpler "double-pole" form of the wave number (Zweig and Shera, 1995; Shera, 2001) in which the parameter values $\{\delta,\rho,\mu\}$ are determined by requiring that the two poles of the BM admittance principally responsible for the peak in the BM velocity response coincide at a given distance, α_*, from the real frequency axis. Formulas for $\{\delta,\rho,\mu\}$ are given in footnote 8 of Shera (2001). For the standard parameters used here we took $\alpha_*=0.06$, yielding $\{\delta,\rho,\mu\}\cong\{-0.063,0.095,1.74\}$. These parameters were chosen to yield $\hat{k}H\cong 6$ for $H\cong 0.7$ mm, in agreement with the estimates from Fig. 1 at 3 kHz. The standard model parameter values are listed in Table I.

TABLE I. Standard model parameter values used in the simulations. Parameter values were chosen to provide rough agreement with Fig. 1 (i.e., $\hat{k}H\cong 6$ at 3 kHz) but may not accurately reproduce other mechanical or otoacoustic responses of the human cochlea. The stimulus frequency (f) and scalae height (H) were sometimes systematically varied from the standard values listed here (e.g., Figs. 10 and 11).

Parameter	Values
f	3.0 kHz
H	0.7 mm
$f_{\mathrm{r}}(0)$	15.0 kHz
$f_{\mathrm{r}}(L)$	2.0 kHz
l	7.0 mm
ρ_0	1.0g/cm^3
b	1.0 mm
N	3.5
α_*	0.06
σ_*	0.005
δ	−0.063
ρ	0.095
μ	1.74
R_{stapes}	0.0
N_x	1500
N_y	100

Mechanical impedance perturbations were introduced by jiggling α_* irregularly with position using random numbers drawn from a Gaussian distribution (with standard a deviation σ_* roughly 1% of the mean). In order to ensure that the mechanical perturbations had no effect on the wave impedances at the ends of the cochlea, the roughness was confined to the central 90% of the cochlear length using a spatial taper.

2. Integrity of the numerical solutions

Simulating OAEs in active cochlear models requires special care. Active models propagate and amplify numerical errors much as they do actual responses to the stimulus. Once they appear, small errors can grow rapidly and thereafter masquerade as genuine otoacoustic responses. Since relative OAE amplitudes are often quite small—human TEOAEs and SFOAEs are typically 10–100 times smaller than the stimulus—computational procedures that suffice when solving solely for the primary response to the stimulus may fail completely when calculating OAEs.

Finite-difference algorithms necessarily discretize the spatial coordinates in the model, and employing too coarse a grid can lead to spurious results. Since the optimal grid spacing depends on both the numerical algorithms employed and the size of the acceptable error, there are no hard and fast rules for determining the number of required sections. In the context of modeling OAEs, an extreme lower bound on N_x might be the number (N_{min}) necessary to represent the spatial frequencies important for emission generation. The theory of coherent reflection filtering yields the estimate $N_{\mathrm{min}}\sim 8L/\hat{\lambda}$ sections, where L is the cochlear length and $\hat{\lambda}$ is the wavelength at the traveling-wave peak for the frequency of interest. The factor of 8 arises as the product 4×2, where the

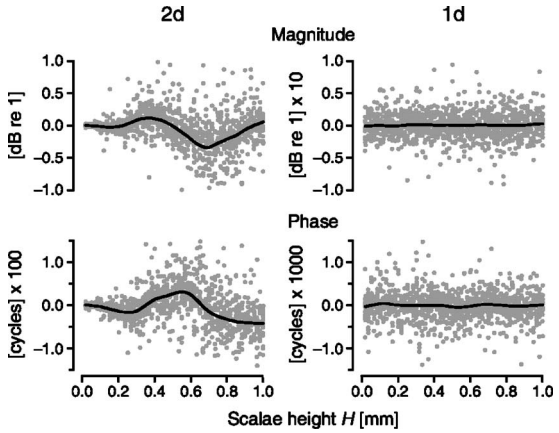

FIG. 17. Scatterplot of the ratio $R_{\mathrm{num}}/R_{\mathrm{Born}}$ in response-matched 1-D and 2-D cochlear models versus scalae height, H. Ratios computed from each of the 2400 simulations used in Fig. 11 are arrayed in four panels: The columns correspond to model dimensionality and the rows to magnitude and phase. The y axes for the 1-D model (column 2) span a range ten times smaller than for the 2-D model. Data points are shown as gray dots and loess trend lines are superposed to guide the eye (Cleveland, 1993). A small percentage of the data (<4%) falls outside the ranges shown.

factor of 4 is needed to encompass the range of spatial frequencies falling within the pass-band of the "spatial-frequency filter" (e.g., Zweig and Shera, 1995, Fig. 6) and the additional factor of 2 arises from Nyquist's sampling theorem. Using estimates of $\hat{\lambda}$ for the human cochlea obtained from measurements of SFOAEs (Shera and Guinan, 2003, Table II) yields $N_{\mathrm{min}}\sim 650$ sections for a model that matches human SFOAE group delays over the full range of human hearing.

Whether any particular grid spacing suffices in practice can only be determined by detailed numerical analysis. Decreasing the grid spacing until the solution no longer varies on scales relevant to the issues at hand often provides a useful empirical assay. Our experience modeling OAEs indicates that the necessary number of sections can sometimes be significantly greater than the lower bound estimated above. To obtain the results reported here we used a longitudinal grid spacing roughly five times finer than L/N_{min}. [To speed up the calculations we truncated our model ($L\cong 14$ mm) so that it did not represent the full range of CFs typical of a healthy human ear. The numbers of sections we employed in the horizontal and vertical directions (N_x and N_y) are given in Table I.] For the 2-D calculations we employed a vertical spacing (H/N_y) similar to that used in the longitudinal direction. In all cases we verified that the solution did not change—at least on the scales relevant here—when the grid spacing was decreased further.

In addition, we checked the accuracy of our numerical procedures by comparing with approximate analytical results (e.g., perturbative calculations of R, WKB approximations for $W_{\{r,l\}}$, etc.) whenever possible. For example, Fig. 17 shows a scatterplot of the ratio $R_{\mathrm{num}}/R_{\mathrm{Born}}$ for each of the 2×1200 simulations reported in Fig. 11. R_{num} is the reflectance computed numerically by solving Laplace's equation (in 2-D) or the Helmholtz equation (in 1-D) using finite-differences (e.g., Neely, 1981; Watts, 2000); R_{Born} is the first-order perturbative expression given by Eq. (45). Quantitative agreement between the methods is generally excellent, with mean ratios indistinguishable from 1 and interquartile ranges for the 2-D model less than 0.25 dB in magnitude and 0.005 cycles in phase (and at least an order of magnitude smaller for the 1-D model). Interestingly, the 2-D scatterplot reveals systematic oscillations with H that appear roughly 90° out of phase in the magnitude and phase plots. These deviations presumably result from small errors in approximation (41) for $\bar{G}_0(x'|x')$ and/or the influence of higher-order nonpropagating pressure modes in the finite-difference solution.

APPENDIX E: FREQUENTLY USED SYMBOLS

Independent variables

x, x', x''	longitudinal distance from stapes
y	vertical distance from BM
ω	$2\pi\times$stimulus frequency, f

Cochlear parameters and maps

H	scalae height
b	BM width
L	cochlear length
ρ_0	density of cochlear fluids
$\mathrm{CF}(x)$	characteristic frequency for location x
$\hat{x}(\omega)$	characteristic place for stimulus frequency ω

Cochlear impedances

$Z_{\mathrm{f}}(\omega)$	fluid acoustic impedance (per unit length) [Eq. (8)]
$\tilde{Z}_{\mathrm{BM}}(x,\omega)$	BM acoustic impedance (times unit length) with perturbations [Eq. (10)]
$Z_{\mathrm{BM}}(x,\omega)$	"smooth" BM impedance without perturbations [Eq. (12)]
$Z^{\mathrm{1d}}_{\mathrm{BM}}(x,\omega)$	BM impedance in response-matched 1-D model
$Z^{\mathrm{2d}}_{\mathrm{BM}}(x,\omega)$	BM impedance in response-matched 2-D model

Dynamical variables

$P(x,y,\omega)$	scalae difference pressure [Eq. (1)]
$U(x,\omega)$	longitudinal component of fluid volume velocity [Eq. (4)]
$U_{\mathrm{ow}}(\omega)$	volume velocity of oval window [Eq. (4)]
$V_{\mathrm{BM}}(x,\omega)$	BM velocity [Eq. (3)]

Wave numbers and wavelengths

$\tilde{k}_{\mathrm{lw}}(x,\omega)$	long-wave wave number with perturbations [Eq. (17)]
$\tilde{k}(x,\omega)$	wave number with perturbations [Eq. (20)]
$k(x,\omega)$	smooth wave number [Eq. (21)]
$\hat{\lambda}(\omega)$	wavelength at $\hat{x}$
$\hat{k}(\omega)$	wave number at $\hat{x}$

Mechanical perturbations

$\Delta Z_{\mathrm{BM}}(x,\omega)$	BM impedance perturbations [Eq. (12)]
$\epsilon(x,\omega)$	fractional wave number perturbations [Eq. (21)]
$\varrho(x,\omega)$	wave number perturbations ϵk^2 [Eq. (29)]

Derived variables

$\bar{P}(x,\omega)$	difference pressure $P(x,y)$ averaged over y [Eq. (7)]
$P_0(x,\omega)$	difference pressure $P(x,0^+)$ across BM [Eq. (16)]
$\alpha(x,\omega)$	pressure ratio $P_0(x)/\bar{P}(x)$ [Eq. (18)]
$\alpha_{\mathrm{WKBs}}(x,\omega)$	α from standard WKB approximation for $P(x,y)$ [Eq. (52)]
$T(x,\omega)$	BM velocity transfer function $V_{\mathrm{BM}}/V_{\mathrm{stapes}}$

Wave components

$W_{\{r,l\}}(x,\omega)$	forward- and reverse-traveling (right- and left-moving) basis waves [Eq. (23)]
$\hat{P}_{\{r,l\}}(x,\omega)$	wave projection operators [Eq. (24)]
$\bar{P}_{\{r,l\}}(x,\omega)$	forward- and reverse-traveling waves
$\bar{P}_0(\omega)$	amplitude of forward-traveling wave at stapes, $\bar{P}_r(0)$
$C_{\{r,l\}}(x,\omega)$	wave coefficients[4]

Green's functions

$G(x,y\|x',y';\omega)$	2D hydrodynamic Green's function [Eq. (26)]
$\bar{G}_0(x\|x';\omega)$	reduced traveling-wave Green's function [Eq. (30)]
$Q(y;x\|y';x',\omega)$	2D Green's function with traveling-wave dependence factored out [Eq. (36)]
$G(x\|x';\omega)$	long-wave traveling-wave Green's function [Eq. (37) and Appendix B]
$G_\infty(x\|x';\omega)$	long-wave traveling-wave Green's function for "infinite" cochlea [Eq. (42)]

Reflectances

$R(\omega)$	apical looking cochlear reflectance [Eq. (13)]
$R_{1\mathrm{d}}(\omega)$	cochlear reflectance in response-matched 1-D model
$R_{2\mathrm{d}}(\omega)$	cochlear reflectance in response-matched 2-D model
$R_{\mathrm{Born}}(\omega)$	first-order (Born) approximation for R [Eq. (45)]
$R_{\mathrm{stapes}}(\omega)$	stapes reflection coefficient

Group delays

$\tau_{\mathrm{BM}}(\omega)$	BM group delay, $-\partial_\omega T$
$\tau(\omega)$	reflectance group delay, $-\partial_\omega R$
$\tau_{1\mathrm{d}}(\omega)$	reflectance group delay in response-matched 1-D model
$\tau_{2\mathrm{d}}(\omega)$	reflectance group delay in response-matched 2-D model

Miscellaneous

$\delta(x)$	Dirac delta function [Eq. (26)]
$\Delta(f,g)$	Wronskian determinant of functions f and g [Eq. (B5)]
γ	reciprocal of Δ [Eq. (B7)]

[1]Informal discussions at the 2002 workshop on the Biophysics of the Cochlea: From Molecules to Models held in Titisee, Germany.

[2]Solutions to the inverse problem in sensitive preparations indicate that at low and moderate intensities the peak of the traveling wave occurs close to the point where traveling-wave amplification reverses sign and the accumulated power is dumped into the organ of Corti. At this point, $\mathrm{Im}\{k(x)\}$ goes through a negative-going zero-crossing (e.g., Zweig, 1991; de Boer, 1995b), and $\hat{k}$ is therefore essentially real.

[3]Our general argument is corroborated by the observation that the approximate analytic expression for $\alpha(x)$ obtained using the WKB approximation[7] applies equally to waves traveling in either direction.

[4]Behind the curtain, the projection operators work by finding the coefficient functions $C_{\{r,l\}}(x)$ needed to write $\bar{P}(x)$ in the form

$$\bar{P}(x)=\underbrace{C_r(x)W_r(x)}_{\bar{P}_r(x)}+\underbrace{C_l(x)W_l(x)}_{\bar{P}_l(x)},$$

where $\bar{P}(x)$ and its first derivative [proportional to U by Eq. (6)] are matched exactly at every point. In other words, the coefficient functions $C_{\{r,l\}}(x)$ are the solutions to the pair of simultaneous equations

$$\bar{P}(x)=C_r(x)W_r(x)+C_l(x)W_l(x),$$

$$\partial_x\bar{P}(x)=C_r(x)\partial_xW_r(x)+C_l(x)\partial_xW_l(x).$$

Solving these equations for the $C_{\{r,l\}}(x)$ and computing the products $\bar{P}_{\{r,l\}}(x)\equiv C_{\{r,l\}}(x)W_{\{r,l\}}(x)$ yields Eqs. (24) and (25). Because they enforce a certain continuous intimacy with the solution, the coefficient functions $C_{\{r,l\}}(x)$ are known as "osculating parameters" (e.g., Mathews and Walker, 1964; Shera and Zweig, 1991; Talmadge *et al.*, 1998).

[5]After Max Born, who derived an analogous expansion in the context of the quantum mechanical theory of collisions (e.g, Born, 1926; Born and Wolf, 1959).

[6]In previous derivations based on the 1-D model (e.g., Shera and Zweig, 1991; Zweig and Shera, 1995; Talmadge *et al.*, 1998, 2000) we solved the scattering problem using a method known as "variation of parameters" (e.g., Mathews and Walker, 1964). The 1-D results can also be derived using a mathematically equivalent procedure based on the long-wave Green's function.

[7]In the standard WKB approximation for the 2-D model (e.g., Steele and Taber, 1979; Viergever, 1980; de Boer and Viergever, 1982), the pressure $P(x,y)$ has the form

$$P_{\mathrm{WKBs}}(x,y)=P_0(x)\,\frac{\cosh[k(x)(H-y)]}{\cosh[k(x)H]}.$$

Calculating $\bar{P}_{\mathrm{WKBs}}(x)$ by averaging this expression over y yields Eq. (52) for $\alpha_{\mathrm{WKBs}}(x)$.

[8]A region of net negative BM resistance near the base of the cochlea is a feature of the Zweig model, which was derived by finding an analytic approximation to the wave number obtained using the inverse method. Note, however, that the uncertainty in the inverse solution is largest in the tail of the response, where the BM velocity response is relatively insensitive to the precise value of the BM resistance.

[9]For clarity we note that the responses of the 1-D model were obtained by solving the 1-D equations—derived by assuming that the pressure is nearly uniform over the scalae—using the specified values of H. Thus, both the 1-D and 2-D models used the same impedances Z_{f} and manifest identical values of $\hat{k}H$.

[10]More explicitly, if $\angle k=\mathrm{atan}(k_i/k_r)$, where k_r and k_i are the real and imaginary parts of k, then $\partial_x\angle k\cong(k_r/|k|^2)\partial_xk_i$, where we have assumed that $k_i\partial_xk_r\cong 0$ because of the zero-crossing in k_i near the peak at $\hat{x}$ (see footnote 2). Scaling implies that spatial derivatives at fixed frequency have the same sign as frequency derivatives at fixed position ($\partial_x/\partial_\omega>0$). Thus, if $k_r>0$ and $\partial_xk_i<0$ near the peak, then $\hat{\tau}_k=-\partial_\omega\angle k>0$.

[11]For an historical introduction to Green and his many functions, see the recent review by Challis and Sheard (2003).

[12]In the short-wave regime, $\alpha\cong kH$ so that the effective scalae height $H_{\mathrm{eff}}\equiv H/\alpha\to 1/k$. Thus $H_{\mathrm{eff}}\cong\hat{\lambda}/2\pi$ near the characteristic place.

[13]According to standard transmission-line theory (with the identification $Z\leftarrow Z_{\mathrm{f}}$), the wave number of the waves on the line is given by $k=\sqrt{-ZY}$ and the characteristic impedance by $Z_0=\sqrt{Z/Y}$ (e.g., Slater, 1942).

[14]In contrast, $Z_0 \rightarrow iZ_{\mathrm{BM}}/H$ when α modifies the shunt admittance.

[15]Zwislocki's (1983) proof is based on a wave equation for the difference pressure $P_0(x)$ obtained using an averaging procedure similar to that of Duifhuis (1988). Rather than average the pressure, Zwislocki (1953) integrates the x derivative of the longitudinal component of the fluid particle velocity over the scalae to obtain an effective cross-sectional area, $q(x)$, defined by the equation $q(x) \equiv S\partial_x \bar{u}/\partial_x u_0$, where $u_0(x) \equiv u(x,0)$ and $u(x,y)$ is the x-component of the fluid particle velocity. Zwislocki (1983) then deduces the transmission-line equations corresponding to the resulting wave equation by intuitively (but mistakenly) associating $q(x)$ with the series impedance characterizing the longitudinal inertia of the fluids. [By following Zwislocki and neglecting small derivatives one can show that $q(x) \cong S/\alpha(x)$.] However, the actual transmission-line equations corresponding to Zwislocki's wave equation are $\partial_x P_0 = -2i\omega\rho u_0$ and $\partial_x u_0 = -P_0/qZ_{\mathrm{BM}}$. In the correct equations, the effective cross-sectional area, proportional to $1/\alpha(x)$, is associated with the BM impedance, just as it is in Fig. 14.

[16]Our terminology derives from de Boer, who refers to the process of deriving the BM impedance with one model and resynthesizing the response with another as "cross-fertilization" (de Boer and Nuttall, 2000).

[17]The various practical complications include (1) transforming frequency-domain responses measured at fixed location $[V_{\mathrm{BM}}(x_0,\omega)]$ into spatial responses measured at fixed frequency $[V_{\mathrm{BM}}(x,\omega_0)]$, as required for use in Eq. (50); (2) minimizing and handling uncertainty due to measurement errors; (3) smoothing the measurements to reduce effects of noise and internal reflection; (4) interpolating and extrapolating to estimate values of V_{BM} at points where measurements are not available; and (5) enforcing known (or presumed) constraints on the functions V_{BM} and k^2 (e.g., causality, minimum-phase behavior, smoothness, asymptotic form at low and high frequencies and/or in extreme basal and apical regions of the cochlea).

[18]To illustrate the d'Alembert formula, consider the wave equation with constant wave number, k_0, and take $W_r(x)$ equal to the forward-traveling wave, e^{-ik_0x}. Equation (A1) for $W_l(x)$ with nonzero $\Delta = 2ik_0(1+\delta)$ then gives

$$W_l(x) = (1+\delta)e^{+ik_0x} - \delta e^{-ik_0x}.$$

When $\delta = 0$, the formula for $W_l(x)$ yields a pure reverse-traveling wave, e^{+ik_0x}; any other value ($\delta \neq -1$) yields a mixture of forward and reverse waves.

[19]Shera and Zweig (1991) show that using the characteristic impedance rather than the retrograde wave impedance can produce large reflections from the stapes (e.g., $|R_{\mathrm{stapes}}| > 0.5$ in Fig. 5 of the 1991 paper). Although terminating the system in its characteristic impedance would eliminate boundary reflection in a uniform transmission line, it does not do so in a nonuniform system where the characteristic impedance varies with position (e.g., a box model of the cochlea).

[20]The procedure for finding $G(x|x')$ outlined here is essentially the same as that used to find the response to a sinusoidal force applied to BM, as described in words in Shera *et al.* [2004, Eq. (1) and surrounding text].

[21]Note that

$$\Delta(w_a,w_b) \equiv \det\begin{pmatrix} w_a & w_b \\ w_a' & w_b' \end{pmatrix} = \det\left[\begin{pmatrix} W_r & W_l \\ W_r' & W_l' \end{pmatrix}\begin{pmatrix} a_r & b_r \\ a_l & b_l \end{pmatrix}\right] = (a_rb_l - a_lb_r)\Delta(W_r,W_l).$$

Evaluating $\Delta(W_r,W_l)$ using the approximate WKB forms $W_{\{r,l\}}^{\mathrm{WKB}}(x)$ given in Eq. (A3) yields $1/\gamma_{\mathrm{WKB}}(\omega) \equiv \Delta(W_r^{\mathrm{WKB}}, W_l^{\mathrm{WKB}}) = 2ik_0(\omega)$.

Allen, J. B. (**1977**). "Two-dimensional cochlear fluid model: New results," J. Acoust. Soc. Am. **61**, 110–119.

Bender, C. M., and Orszag, S. A. (**1978**). *Advanced Mathematical Methods for Scientists and Engineers* (McGraw-Hill, New York).

Beranek, L. L. (**1986**). *Acoustics* (American Institute of Physics, New York).

Born, M. (**1926**). "Quantenmechanik der Stossvorgänge (Quantum mechanics of impact processes)," Z. Phys. **38**, 803–827.

Born, M., and Wolf, E. (**1959**). *Principles of Optics: Electromagnetic Theory of Propagation, Interference and Diffraction of Light* (Pergamon, Oxford).

Bredberg, G. (**1968**). "Cellular patterns and nerve supply of the human organ of Corti," Acta Oto-Laryngol., Suppl. **236**, 1–135.

Carlin, H. J., and Giordano, A. B. (**1964**). *Newtork Theory: An Introduction to Reciprocal and Nonreciprocal Circuits* (Prentice Hall, Englewood Cliffs, NJ).

Challis, L., and Sheard, F. (**2003**). "The Green of Green functions," Phys. Today **56**, 41–46.

Cleveland, W. S. (**1993**). *Visualizing Data* (Summit Hobart, NJ).

Cooper, N. P., and Shera, C. A. (**2004**). "Backward traveling waves in the cochlea? Comparing basilar membrane vibrations and otoacoustic emissions from individual guinea-pig ears," Assoc. Res. Otolaryngol. Abs. **27**, 1008.

Courant, R. (**1988**). *Differential and Integral Calculus, Vol. II* (Wiley Interscience, New York).

Courant, R., and Hilbert, D. (**1953**). *Methods of Mathematical Physics* (Wiley Interscience, New York).

de Boer, E. (**1979**). "Short-wave world revisited: Resonance in a two-dimensional cochlear model," Hear. Res. **1**, 253–281.

de Boer, E. (**1983**). "Wave reflection in passive and active cochlea models," in *Mechanics of Hearing*, edited by E. de Boer and M. A. Viergever (Martinus Nijhoff, The Hague), pp. 135–142.

de Boer, E. (**1995a**). "The inverse problem solved for a three-dimensional model of the cochlea. I. Analysis," J. Acoust. Soc. Am. **98**, 896–903.

de Boer, E. (**1995b**). "The inverse problem solved for a three-dimensional model of the cochlea. II. Application to experimental data sets," J. Acoust. Soc. Am. **98**, 904–910.

de Boer, E. (**1996**). "Mechanics of the cochlea: Modeling efforts," in *The Cochlea*, edited by P. Dallos, A. N. Popper, and R. R. Fay (Springer-Verlag, New York), pp. 258–317.

de Boer, E. (**2001**). "The short-wave model and waves in two directions," J. Acoust. Soc. Am. **109**, 291–293.

de Boer, E., and Nuttall, A. L. (**1999**). "The inverse problem solved for a three-dimensional model of the cochlea. III. Brushing-up the solution method," J. Acoust. Soc. Am. **105**, 3410–3420.

de Boer, E., and Nuttall, A. L. (**2000**). "The mechanical waveform of the basilar membrane. II. From data to models—and back," J. Acoust. Soc. Am. **107**, 1487–1496.

de Boer, E., and Viergever, M. A. (**1982**). "Validity of the Liouville-Green (or WKB) method for cochlear mechanics," Hear. Res. **8**, 131–155.

de Boer, E., and Viergever, M. A. (**1984**). "Wave propagation and dispersion in the cochlea," Hear. Res. **13**, 101–112.

de Boer, E., Nuttall, A. L., and Grosh, K. (**2004**). "Elusive entrainment," Assoc. Res. Otolaryngol. Abs. **27**, 544.

Dhar, S., Talmadge, C. L., Long, G. R., and Tubis, A. (**2002**). "Multiple internal reflections in the cochlea and their effect on DPOAE fine structure," J. Acoust. Soc. Am. **112**, 2882–2897.

Duifhuis, H. (**1988**). "Cochlear macromechanics," in *Auditory Function: Neurological Bases for Hearing*, edited by G. M. Edelman, W. E. Gall, and W. M. Cowan (Wiley, New York), pp. 189–212.

Dunford, N., and Schwartz, J. T. (**1971**). *Linear Operators, Part III* (Wiley, New York).

Engström, H., Ades, H. W., and Andersson, A. (**1966**). *Structural Pattern of the Organ of Corti* (Williams and Wilkins, Baltimore).

Friedman, B. (**1956**). *Principles and Techniques of Applied Mathematics* (Wiley, New York).

Fröman, N., and Fröman, P. O. (**1965**). *JWKB Approximation: Contributions to the Theory* (North-Holland, Amsterdam).

Gould, S. J., and Lewontin, R. C. (**1979**). "The spandrels of San Marco and the Panglossian paradigm: a critique of the adaptationist programme," Proc. R. Soc. London, Ser. B **205**, 581–598.

Greenwood, D. D. (**1961**). "Critical bandwidth and the frequency coordinates of the basilar membrane," J. Acoust. Soc. Am. **33**, 1344–1356.

Greenwood, D. D. (**1990**). "A cochlear frequency-position function for several species—29 years later," J. Acoust. Soc. Am. **87**, 2592–2605.

Hubbard, A. E., and Mountain, D. C. (**1996**). "Analysis and synthesis of cochlear mechanical function using models," in *Auditory Computation*, edited by H. L. Hawkins, T. A. McMullen, A. N. Popper, and R. R. Fay (Springer-Verlag, New York), pp. 62–120.

Ince, E. L. (**1956**). *Ordinary Differential Equations* (Dover, New York).

Jay, R. (**2001**). *Jay's Journal of Anomalies: Conjurers, Cheats, Hustlers, Hoaxsters, Pranksters, Jokesters, Imposters, Pretenders, Side-Show Showmen, Armless Calligraphers, Mechanical Marvels, Popular Entertainments* (Farrar Straus & Giroux, New York).

Kemp, D. T., and Brown, A. M. (**1983**). "An integrated view of cochlear mechanical non-linearities observable from the ear canal," in *Mechanics*

of Hearing, edited by E. de Boer and M. A. Viergever (Martinus Nijhoff, The Hague), pp. 75–82.
Lighthill, J. (**1981**). "Energy flow in the cochlea," J. Fluid Mech. **106**, 149–213.
Lonsbury-Martin, B. L., Martin, G. K., Probst, R., and Coats, A. C. (**1988**). "Spontaneous otoacoustic emissions in the nonhuman primate. II. Cochlear anatomy," Hear. Res. **33**, 69–94.
Mammano, F., and Nobili, R. (**1993**). "Biophysics of the cochlea: Linear approximation," J. Acoust. Soc. Am. **93**, 3320–3332.
Mathews, J., and Walker, R. (**1964**). *Mathematical Methods of Physics* (Benjamin, New York).
Morse, P. M., and Feshbach, H. (**1953**). *Methods of Theoretical Physics, Parts I and II* (McGraw-Hill, New York).
Nedzelnitsky, V. (**1980**). "Sound pressures in the basal turn of the cat cochlea," J. Acoust. Soc. Am. **68**, 1676–1689.
Neely, S. T. (**1981**). "Finite difference solution of a two-dimensional mathematical model of the cochlea," J. Acoust. Soc. Am. **69**, 1386–1393.
Olson, E. S. (**2001**). "Intracochlear pressure measurements related to cochlear tuning," J. Acoust. Soc. Am. **110**, 349–367.
Oxenham, A. J., and Shera, C. A. (**2003**). "Estimates of human cochlear tuning at low levels using forward and simultaneous masking," J. Assoc. Res. Otolaryngol. **4**, 541–554.
Parthasarathi, A. A., Grosh, K., and Nuttall, A. L. (**2000**). "Three-dimensional numerical modeling for global cochlear dynamics," J. Acoust. Soc. Am. **107**, 474–485.
Peake, W. T., Rosowski, J. J., and Lynch, T. J. (**1992**). "Middle-ear transmission: Acoustic versus ossicular coupling in cat and human," Hear. Res. **57**, 245–268.
Peterson, L. C., and Bogert, B. P. (**1950**). "A dynamical theory of the cochlea," J. Acoust. Soc. Am. **22**, 369–381.
Probst, R., Lonsbury-Martin, B. L., and Martin, G. K. (**1991**). "A review of otoacoustic emissions," J. Acoust. Soc. Am. **89**, 2027–2067.
Puria, S. (**2003**). "Measurements of human middle ear forward and reverse acoustics: Implications for otoacoustic emissions," J. Acoust. Soc. Am. **113**, 2773–2789.
Ren, T. (**2002**). "Longitudinal pattern of basilar membrane vibration in the sensitive cochlea," Proc. Natl. Acad. Sci. U.S.A. **99**, 17101–17106.
Ren, T. (**2004**). "Reverse propagation of sound in the gerbil cochlea," Nat. Neurosci. **7**, 333–334.
Ruggero, M. A. (**2004**). "Comparison of group delays of $2f_1-f_2$ distortion product otoacoustic emissions and cochlear travel times," ARLO **5**, 143–147.
Schairer, K. S., Fitzpatrick, D., and Keefe, D. H. (**2003**). "Input-output functions for stimulus-frequency otoacoustic emissions in normal-hearing adult ears," J. Acoust. Soc. Am. **114**, 944–966.
Shera, C. A. (**2001**). "Intensity-invariance of fine time structure in basilar-membrane click responses: Implications for cochlear mechanics," J. Acoust. Soc. Am. **110**, 332–348.
Shera, C. A. (**2003a**). "Mammalian spontaneous otoacoustic emissions are amplitude-stabilized cochlear standing waves," J. Acoust. Soc. Am. **114**, 244–262.
Shera, C. A. (**2003b**). "Wave interference in the generation of reflection- and distortion-source emissions," in *Biophysics of the Cochlea: From Molecules to Models*, edited by A. W. Gummer (World Scientific, Singapore), pp. 439–453.
Shera, C. A., and Guinan, J. J. (**1999**). "Evoked otoacoustic emissions arise by two fundamentally different mechanisms: A taxonomy for mammalian OAEs," J. Acoust. Soc. Am. **105**, 782–798.
Shera, C. A., and Guinan, J. J. (**2003**). "Stimulus-frequency-emission group delay: A test of coherent reflection filtering and a window on cochlear tuning," J. Acoust. Soc. Am. **113**, 2762–2772.
Shera, C. A., and Zweig, G. (**1991**). "Reflection of retrograde waves within the cochlea and at the stapes," J. Acoust. Soc. Am. **89**, 1290–1305.
Shera, C. A., and Zweig, G. (**1992a**). "Analyzing reverse middle-ear transmission: Noninvasive Gedanken experiments," J. Acoust. Soc. Am. **92**, 1371–1381.
Shera, C. A., and Zweig, G. (**1992b**). "An empirical bound on the compressibility of the cochlea," J. Acoust. Soc. Am. **92**, 1382–1388.
Shera, C. A., and Zweig, G. (**1992c**). "Middle-ear phenomenology: The view from the three windows," J. Acoust. Soc. Am. **92**, 1356–1370.
Shera, C. A., and Zweig, G. (**1993a**). "Noninvasive measurement of the cochlear traveling-wave ratio," J. Acoust. Soc. Am. **93**, 3333–3352.
Shera, C. A., and Zweig, G. (**1993b**). "Order from chaos: Resolving the paradox of periodicity in evoked otoacoustic emission," in *Biophysics of Hair Cell Sensory Systems*, edited by H. Duifhuis, J. W. Horst, P. van Dijk, and S. M. van Netten (World Scientific, Singapore), pp. 54–63.
Shera, C. A., Guinan, J. J., and Oxenham, A. J. (**2002**). "Revised estimates of human cochlear tuning from otoacoustic and behavioral measurements," Proc. Natl. Acad. Sci. U.S.A. **99**, 3318–3323.
Shera, C. A., Talmadge, C. L., and Tubis, A. (**2000**). "Interrelations among distortion-product phase-gradient delays: Their connection to scaling symmetry and its breaking," J. Acoust. Soc. Am. **108**, 2933–2948.
Shera, C. A., Tubis, A., and Talmadge, C. L. (**2004**). "Are there forward and reverse traveling waves in the cochlea? Countering the critique of Nobili *et al.*," J. Assoc. Res. Otolaryngol. **5**, 349–359.
Shera, C. A., Tubis, A., and Talmadge, C. L. (**2005**). "Coherent-reflection models of reflection-source OAEs with and without slow transverse retrograde waves," Assoc. Res. Otolaryngol. Abs. **28**, 657.
Siebert, W. M. (**1974**). "Ranke revisited—a simple short-wave cochlear model," J. Acoust. Soc. Am. **56**, 594–600.
Slater, J. C. (**1942**). *Microwave Transmission* (McGraw-Hill, New York).
Steele, C. R., and Taber, L. A. (**1979**). "Comparison of WKB and finite difference calculations for a two-dimensional cochlear model," J. Acoust. Soc. Am. **65**, 1001–1006.
Talmadge, C. L., Tubis, A., and Tong, C. (**2001**). "Cochlear wave reflection due to roughness in 2-D and 3-D cochlear models," Assoc. Res. Otolaryngol. Abs. **24**, 44.
Talmadge, C. L., Tubis, A., Long, G. R., and Piskorski, P. (**1998**). "Modeling otoacoustic emission and hearing threshold fine structures," J. Acoust. Soc. Am. **104**, 1517–1543.
Talmadge, C. L., Tubis, A., Long, G. R., and Tong, C. (**2000**). "Modeling the combined effects of basilar membrane nonlinearity and roughness on stimulus frequency otoacoustic emission fine structure," J. Acoust. Soc. Am. **108**, 2911–2932.
Thorne, M., Salt, A. N., DeMott, J. E., Henson, M. M., Henson, O. W., and Gewalt, S. L. (**1999**). "Cochlear fluid space dimensions for six species derived from reconstructions of three-dimensional magnetic resonance images," Laryngoscope **109**, 1661–1668.
Viergever, M. A. (**1980**). *Mechanics of the Inner Ear: A Mathematical Approach* (Delft U.P., Delft).
Viergever, M. A., and de Boer, E. (**1987**). "Matching impedance of a non-uniform transmission line: Application to cochlear modeling," J. Acoust. Soc. Am. **81**, 184–186.
Voss, S. E., Rosowski, J. J., and Peake, W. T. (**1996**). "Is the pressure difference between the oval and round window the effective stimulus for the cochlea?" J. Acoust. Soc. Am. **100**, 1602–1616.
Watts, L. (**1992**). *Cochlear Mechanics: Analysis and Analog VLSI*, Ph.D. thesis, California Institute of Technology.
Watts, L. (**2000**). "The mode-coupling Liouville-Green approximation for a two-dimensional cochlear model," J. Acoust. Soc. Am. **108**, 2266–2271.
Wegel, R. L., and Lane, C. E. (**1924**). "The auditory masking of one pure tone by another and its probable relation to the dynamics of the inner ear," Phys. Rev. **23**, 266–285.
Wilson, J. P. (**1980**). "Model for cochlear echoes and tinnitus based on an observed electrical correlate," Hear. Res. **2**, 527–532.
Wright, A. A. (**1984**). "Dimensions of the cochlear stereocilia in man and in guinea pig," Hear. Res. **13**, 89–98.
Zurek, P. M. (**1985**). "Acoustic emissions from the ear: A summary of results from humans and animals," J. Acoust. Soc. Am. **78**, 340–344.
Zweig, G. (**1976**). "Basilar membrane motion," in *Cold Spring Harbor Symposia on Quantitative Biology, volume XL, 1975* (Cold Spring Harbor Laboratory, Cold Spring Harbor), pp. 619–633.
Zweig, G. (**1991**). "Finding the impedance of the organ of Corti," J. Acoust. Soc. Am. **89**, 1229–1254.
Zweig, G., and Shera, C. A. (**1995**). "The origin of periodicity in the spectrum of evoked otoacoustic emissions," J. Acoust. Soc. Am. **98**, 2018–2047.
Zweig, G., Lipes, R., and Pierce, J. R. (**1976**). "The cochlear compromise," J. Acoust. Soc. Am. **59**, 975–982.
Zwislocki, J. (**1953**). "Wave motion in the cochlea caused by bone conduction," J. Acoust. Soc. Am. **25**, 986–989.
Zwislocki, J. J. (**1983**). "Sharp vibration maximum in the cochlea without wave reflection," Hear. Res. **9**, 103–111.
Zwislocki, J. J. (**2002**). *Auditory Sound Transmission: An Autobiographical Perspective* (Erlbaum, Mahwah, NJ).
Zwislocki-Mośćicki, J. (**1948**). "Theorie der Schneckenmechanik: Qualitative und Quantitative Analysis," Acta Oto-Laryngol., Suppl. **72**, 1–112.